9-2015

Ordering and topological defects in solids with quenched randomness

Thomas Chapman Proctor
Graduate Center, City University of New York

Ordering and topological defects in solids with quenched randomness

by

Thomas Chapman Proctor

A dissertation submitted to the Graduate Faculty in Physics in partial fulfillment of the requirements for the degree of Doctor of Philosophy, The City University of New York

2015

This manuscript has been read and accepted for the Graduate Faculty in Physics in satisfaction of the dissertation requirement for the degree of Doctor of Philosophy.

Prof. Igor Kuskovsky

Date | Executive Officer

Dist. Prof. Eugene M. Chudnovsky

Date | Chair of Examining Committee

Prof. Dmitry A. Garanin | **Prof. Andrew Kent**

Prof. Vadim Oganesyan | **Dist. Prof. Myriam P. Sarachik**

Supervisory Committee

The City University of New York

Abstract

Ordering and topological defects in solids with quenched randomness

by

Thomas Chapman Proctor

Adviser: Professor Eugene M. Chudnovsky

We explore multiple different examples of quenched randomness in systems with a continuous order parameter. In all these systems, it is shown that understanding the effects of topology is critical to the understanding of the effects of quenched randomness.

We consider n-component fixed-length order parameter interacting with a weak random field in $d = 1, 2, 3$ dimensions. Relaxation from the initially ordered state and spin-spin correlation functions have been studied on lattices containing hundreds of millions sites. At $n - 1 < d$ presence of topological structures leads to metastability, with the final state depending on the initial condition. At $n - 1 > d$, when topological objects are absent, the final, lowest-energy, state is independent of the initial condition. It is characterized by the exponential decay of correlations that agrees quantitatively with the theory based upon the Imry-Ma argument. In the borderline case of $n - 1 = d$, when topological structures are non-singular, the system possesses a weak metastability with the Imry-Ma state likely to be the global energy minimum.

We study random-field xy spin model at $T = 0$ numerically on lattices of up to $1000 \times 1000 \times 1000$ spins with the accent on the weak random field. Our numerical method is physically equivalent to slow cooling in which the system is gradually losing the energy and relaxing to an energy minimum. The system shows glass properties, the resulting spin states depending strongly on the initial conditions. Random initial condition for the spins leads to the vortex glass (VG) state with short-range spin-spin correlations defined by the average

distance between vortex lines. Collinear and some other vortex-free initial conditions result in the vortex-free ferromagnetic (F) states that have a lower energy. The energy difference between the F and VG states correlates with vorticity of the VG state. Correlation functions in the F states agree with the Larkin-Imry-Ma theory at short distances. Hysteresis curves for weak random field are dominated by topologically stable spin walls raptured by vortex loops. We find no relaxation paths from the F, VG, or any other states to the hypothetical vortex-free state with zero magnetization.

XY and Heisenberg spins, subjected to strong random fields acting at few points in space with concentration $c_r \ll 1$, are studied numerically on 3d lattices containing over four million sites. Glassy behavior with strong dependence on initial conditions is found. Beginning with a random initial orientation of spins, the system evolves into ferromagnetic domains inversely proportional to c_r in size. The area of the hysteresis loop, $m(H)$, scales as c_r^2. These findings are explained by mapping the effect of strong dilute random field onto the effect of weak continuous random field. Our theory applies directly to ferromagnets with magnetic impurities, and is conceptually relevant to strongly pinned vortex lattices in superconductors and pinned charge density waves.

The random-anisotropy Heisenberg model is numerically studied on lattices containing over ten million spins. The study is focused on hysteresis and metastability due to topological defects, and is relevant to magnetic properties of amorphous and sintered magnets. We are interested in the limit when ferromagnetic correlations extend beyond the size of the grain inside which the magnetic anisotropy axes are correlated. In that limit the coercive field computed numerically roughly scales as the fourth power of the random anisotropy strength and as the sixth power of the grain size. Theoretical arguments are presented that provide an explanation of numerical results. Our findings should be helpful for designing amorphous and nanosintered materials with desired magnetic properties.

Acknowledgments

Without the help of my advisor, Eugene Chudnovsky, this work would surely not have been possible. His knowledge, understanding, and clear and simple explanations of the physics of random magnets have allowed me to grasp the work that has come before me quickly and with ease. His comprehension of the field has allowed him to make the excellent suggestions on problems to pursue which has led to this work. Eugene has always been willing to lend advice, whether on physics or my career, which has helped me immensely.

Just as fundamentally important to this work has been my unofficial second advisor, Dmitry Garanin. Whenever I hit a roadblock in my research, Dmitry was there to help, willing to patiently and critically listen, talk about problems, and make suggestions for paths to follow. This has been invaluable to me, helping me find many new routes to pursue and fortifying my understanding of the problems I struggled with.

My fellow graduate students at Lehman College, Mike O'Keeffe, Liufe Cai, Debajyoti Sarkar, and Ricardo Zarzuela have shared excellent discussions on physics, greatly expanding the scope of my understanding with their expansive knowledge. Mike O'Keeffe has especially helped me with all the practical elements of doing physics research and being a graduate student, from teaching to writing these acknowledgments and much more.

I thank my fellow physicists who frequent the GC Science Center for always being up for interesting physics discussions. While they may have rarely had direct applications to my research, these discussions were always stimulating and exciting, helping both to motivate

me in my work and to think about random magnets in new and interesting ways.

While all of my professors both at Reed College and at CUNY have helped tremendously in my learning and development as a physicist, David Griffiths deserves special mention. His patience and excitement guiding me through my first forays into independent research as my undergraduate thesis advisor opened my eyes to the joys of physics research and awakened my drive to pursue it further.

Finally, I could not have done this without the emotional support of those I love, especially the support of my family. My parents, Judy and Ched, have given wonderful support throughout my academic career and have always encouraged my love of physics. My fiancée Sandra has brought boundless joy and humor into my life which has made the graduate student life we have gone through together happy despite all the stress.

Contents

List of Figures

Chapter 1

Introduction

This thesis hopes to answer some of the questions related the effects of quenched disorder on long range order in a system with a continuous order parameter. While the effect of quenched randomness that strongly interacts with the order parameter is in most cases trivial, the effects of weakly interacting disorder are not obvious and have had a history of controversy and disagreement. In 1970 Larkin[1] first proposed that a random field may be behind amorphous structure in the Abrisokov vortex lattice in type II superconductors. A few years later, Imry and Ma[2] came up with a qualitative argument which extended Larkin's findings to any dimension. They found that a random field will destroy long range order no matter how weak the random field is, as long as the number of dimensions of the system are less than four. They also produced a prediction for the scaling of the finite correlation length with respect to the random field strength for dimensions less than four. Their argument was also sufficiently general that it can be directly applied to random anisotropy systems as well. Aizman and Wehr[3] provided a rigorous proof of Imry and Ma's claim that random fields and anisotropy will destroy ferromagnetic order for dimensions less than four.

Along with these theoretical developments, it was shown that random field and random anisotropy models have multitudes of applications beyond the super conducting systems [4,

5, 6], in which Larkin first encountered them. The random field model has been applied to charge density waves[7–13], disordered antiferromagnets[14], Josephson Junction arrays[15], magnetic bubbles in two-dimensional arrays [16, 17], superfluid .^{3}He-A aerogel [18, 19], amorphous and sintered ferromagnets[20–24]

However, in the 1980s, the validity of the Imry-Ma-Larkin argument was questioned by renormalization group treatments[25–27]. Furthermore, scaling and replica symmetry breaking arguments[13, 28–32], as well as a variational method[33, 34] led to a power-law dependence of correlations at large distances, contradicting the prediction of the destruction of long range order. This quasi-ordered state was named a Bragg glass.

Further complicating the issue, results for decoration[5] and neutron scattering[6] experiments in superconductors have not been conclusive

This thesis hopes to resolve these issues. Our main method is to study various random field and random anisotropy models numerically, by relaxing from an initial state to find a local minima.

In Section 1.1, we present the important argument of Imry and Ma[2], which argues that quenched disorder should destroy long range order in dimmensions less than four.

In Section 1.2 we explain our numerical method and show that it is effective at finding physically relevant states.

In Chapter 2, we have tested a possible explanation for confusing behavior of the random field model: conserved topological structures provide significant energy barriers such that the system is dominated by the metastable states created by these energy barriers. However, these topological structures are dependent on the dimensionality of the system. For a model with nu number of components of the order parameter and d dimensions, conserved topological structures exist if $n \leq d + 1$, however no such topological structures exist for models where $n > d + 1$. By comparing the behavior of models with different n and d, we find metastability in systems where conserved topological structures can exist, but no

metastability for models where there are no such topological structures.

In Chapter 3 we focus on a specific physically relevant model, the random field XY model in three dimensions, i.e. a random field model where $n = 2$ and $d = 3$. We explore the model's behavior under various numerical experiments, and look at the specifics of magnetization, energy, and vortices, the conserved topological structures in this model.

In Chapter 4, we look at a strong random field that only interacts with the order parameter at a few dilute points. We find that this problem can be explained well using the understanding that we have gained from the previous chapters, as the problem can be re-scaled to ones we have previously explored.

In Chapter 5, we look another type of quenched randomness, random anisotropy, which is particularly relevant to micromagnetics. We focus on aspects experimentally relevant to magnetism, correlation functions and hysteresis curves.

1.1 The Imry-Ma-Larkin Argument

Here, we will give a general qualitative statistical argument following the argument of Imry and Ma[2]. For this argument, our energy has an exchange term,

$$\mathcal{E}_{ex} = \int d^d r \, \alpha \left(\frac{\partial \mathbf{S}}{\partial r_i} \frac{\partial \mathbf{S}}{\partial r_j} \right) \tag{1.1}$$

For the sake of this discussion, we will consider $\mathbf{S}(\mathbf{r})$ to be a unitless order parameter. We also have a random potential energy,

$$\mathcal{E}_{ran} = -\beta \int d^d r \, \mathcal{V}_{ran} \left(\mathbf{S}(\mathbf{r}), \mathbf{r} \right) \tag{1.2}$$

where $\mathcal{V}_{ran} \left(\mathbf{S}(\mathbf{r}), \mathbf{r} \right)$ is the unitless portion of a random potential. It is a random function of $\mathbf{r}$ correlated over some length R_a, but not random in $\mathbf{S}(\mathbf{r})$. β is a constant which contains all

quantities in the potential with units, and thus has units of energy density. For the purposes of this discussion, we can remain agnostic to the exact character of $\mathcal{V}_{ran}\left(\mathbf{S}(\mathbf{r}),\mathbf{r}\right)$. Examples we will study in detail in later chapters include a random field given by

$$\mathcal{V}_{ran}\left(\mathbf{S}(\mathbf{r}),\mathbf{r}\right)=\mathbf{h}(\mathbf{r})\cdot\mathbf{S}(\mathbf{r}), \tag{1.3}$$

where $\mathbf{h}(\mathbf{r})$ is a dimensionless vector field of unit length and random direction, and random anisotropy,

$$\mathcal{V}_{ran}\left(\mathbf{S}(\mathbf{r}),\mathbf{r}\right)=\left(\mathbf{n}(\mathbf{r})\cdot\mathbf{S}(\mathbf{r})\right)^{2}, \tag{1.4}$$

where $\mathbf{n}(\mathbf{r})$ is a dimensionless random vector field of unit length.

Important to our discussion is that $\beta R_a^2 \ll \alpha$. Without this condition, behavior of the order parameter is dominated by the random potential and in general much simpler than the problem we will explore here. For example, for the potential given in Eq. (1.3), the order parameter will simply follow the direction of the random field $\mathbf{h}(\mathbf{r})$.

With $\beta \ll \alpha R_a^2$, the result is far from obvious. If the system were to disorder, than the order parameter must be correlated on a scale $R_f \gg R_a$, as disorder on any smaller scale will be prohibited by both strong exchange energy and the random potential. The scaling of the exchange energy over a volume V will be

$$\mathcal{E}_{ex} \propto \alpha\frac{V}{R_f^2}, \tag{1.5}$$

Within the volume over which the order parameter is correlated, R_f^d, the order parameter cannot be well correlated with any local value of the random potential. Over an infinite volume, this would mean that the average contribution to the energy will simply be the mean value independent of the configuration of the order parameter. However, over the finite volume R_f^d, the deviation of the sample average from this mean will be the standard

deviation of the sample average given by the central limit theorem, i.e. $\propto \sqrt{\frac{1}{N}}$, where N is the number of elements in our sample. Within the volume R_f^d, this number is the number of independent random instances of our random potential,

$$N \propto \left(\frac{R_f}{R_a}\right)^d. \tag{1.6}$$

Thus, we expect the energy contribution from the random field to be

$$\mathcal{E}_{ran} \propto -\beta V \left(\frac{R_f}{R_a}\right)^{-d/2}, \tag{1.7}$$

and our total energy is given by

$$\mathcal{E} \propto \alpha \frac{V}{R_f^2} - \beta V \left(\frac{R_f}{R_a}\right)^{-d/2}. \tag{1.8}$$

Extremal values of this energy for R_f are

$$\frac{R_f}{R_a} \propto \left(\frac{\sqrt{\frac{\alpha}{\beta}}}{R_a}\right)^{\frac{4}{4-d}}. \tag{1.9}$$

In order to check to make sure we have found a minimum, we can do the second derivative test, and find

$$\frac{d^2\mathcal{E}}{dR_f^2} = -\frac{(d^2+2d-24)}{4} V \left(\alpha^{-d+4}\beta^8 R_a^{4d}\right)^{\frac{1}{4-d}} \tag{1.10}$$

For $d < 4$, $\frac{d^2\mathcal{E}}{dR_f^2}$ is positive, implying we have found an energy minimum. For $d \geq 4$, $\frac{d^2\mathcal{E}}{dR_f^2}$ we find we have found a maximum or inflection point, and no disordered energy minimum exists. We can then generally state that for $d < 4$, an arbitrarily weak random potential will destroy long range order, while for $d \geq 4$, it will not.

1.1.1 Hysteresis in the Imry-Ma Picture

Based off this information, we can look at the qualitative behavior of any hysteresis that we might observe. While we would not expect hysteresis based off what we have discussed so far, we will see evidence for hysteresis in later chapters. If we treat each Imry-Ma domain independently, we would expect the coercive field to scale with the effective random field of the domain,

$$H_c \propto \beta_{\text{eff}}. \tag{1.11}$$

The effective field β_{eff} will be given by Eq. (1.7), and plugging in Eq. (1.9), we find

$$H_c \propto \beta \left(\frac{R_a}{\sqrt{\frac{\alpha}{\beta}}} \right)^{\frac{2d}{4-d}}. \tag{1.12}$$

It should be mentioned that these results are on valid for $a \leq R_a \ll R_f \ll L$. This is clear from the structure of the argument. If R_a is less than the site separation of the lattice, a, it is no longer meaningful and R_a can be replaced by a. We must have $R_a \ll R_f$, as we require statistical averaging for Eq. (1.7), and $R_f \ll L$ is required or else the system will be dominated by boundary effects.

1.2 The numerical method of relaxation and "over-relaxation"

The task is to find energy minima of a Hamiltonian with quenched randomness by a numerical algorithm starting from an initial state (IC) and using some relaxation protocol. It turns out that there are multitudes of local energy minima and the situation resembles that of a spin glass. At the end of relaxation the system ends up in one of them. We do not attempt

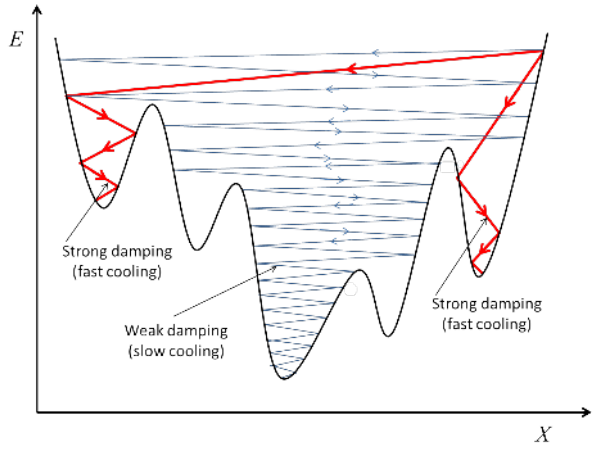

Figure 1.1: Efficiency of the weak-damping (slow-cooling) method for glassy systems.

to search for the ground state of the system, which would require different numerical methods. Rather, we are interested in representative local minima obtained by relaxation from typical IC such as random and collinear initial conditions. This corresponds to experimental situations, and the results for physical quantities in the final state are reproducible up to statistical noise due to different realizations of the random field and different realizations of the relaxation protocol that may have a stochastic part. The larger the system size, the smaller the fluctuations. For smaller sizes, averaging of the results over realizations of the random field is necessary.

One could use the Landau-Lifshitz equation of motion with damping (with no precession term for the xy model) to find local energy minima. One can expect an even faster relaxation if one rotates every spin, sequentially, straight in the direction of the effective magnetic field

$$\mathbf{H}_{i,\text{eff}} = \sum_j J_{ij}\mathbf{s}_j + \mathbf{h}_j + \mathbf{H} \tag{1.13}$$

that is [35]

$$\mathbf{s}_{i,\text{new}} = \mathbf{H}_{i,\text{eff}} / \left|\mathbf{H}_{i,\text{eff}}.\right| \tag{1.14}$$

We call this the finite rotation (FR) method. Although this method works very well in cases when there is only one energy minimum (such as the collinear state for pure ferromagnetic models), it leads to slow relaxation in the case of glassy behavior characterized by many local minima. The problem is that the relaxation described by Eq. (1.14) is initially too fast and the system falls into the nearest local minimum that is not the deepest and not the most representative. As in the multi-dimensional space of our model there are narrow valleys rather than simple local minima, the system quickly falls into one of these valleys and then begins a long travel along it.

To counter this slow relaxation, it is convenient to combine the FR method with so-called over-relaxation [36] that is, in fact, a conservative pseudo-dynamics described by

$$\mathbf{s}_{i,\mathrm{new}} = \frac{2\left(\mathbf{s}_{i,\mathrm{old}} \cdot \mathbf{H}_{i,\mathrm{eff}}\right)\mathbf{H}_{i,\mathrm{eff}}}{H_{i,\mathrm{eff}}^2} - \mathbf{s}_{i,\mathrm{old}}. \tag{1.15}$$

Here spins are sequentially flipped onto the other side of the effective field (half of the precession period for the Heisenberg model) and the energy is conserved. This method is very convenient to quickly explore the hypersurface of constant energy of the system. Whereas the FR method searches for a minimal energy, the over-relaxation method searches for the maximal entropy. It is a standard numerical method for classical spin systems, usually combined with Monte Carlo updates (see, e.g., Ref. [37]).

For instance, starting from the collinear state and using the over-relaxation method, one can describe FR-induced transition of the system from the initial state that has the minimal statistical weight to a more disordered state having the same energy but a much higher statistical weight. This process describes an irreversible relaxation in which the magnetization value m decreases from 1 to a smaller value. The resulting final state is above the ground state, so it can be interpreted as a thermal state with some small temperature. Adding the energy-lowering evolution described by Eq. (1.14) one can find the lowest-energy

state in this particular region of phase space.

Practically it is convenient to combine both methods. In the main method we used, Eq. (1.14) is applied with the probability α while Eq. (1.15) is applied with the probability $1-\alpha$. The optimal value of α that plays the role of a relaxation constant is in the range $0.1-0.01$, typically 0.03. Physically this corresponds to slow cooling the system. Such a choice results in convergence acceleration by factors greater than 10 in comparison to $\alpha = 1$. The efficiency of the combined weak damping method for glassy systems is shown in Fig. 1.1, assuming that deeper minima have broader basins of attraction.

Starting from the collinear state, we also used a two-stage relaxation method. The first stage, which we call "chaotization", is the conservative pseudo-dynamics given by Eq. (1.15). The second stage is the combined relaxation process described above. In some cases during chaotization damped oscillating behavior was observed. In this case suppression of oscillations and a faster convergence can be achieved by performing Eq. (1.15) with a probability $1-\eta$ and leaving the spin unchanged with the probability η. The constant η that has the optimal value about 0.01 plays the role of a decoherence constant in the numerical method.

As we have seen, at $h < Js$, the regions that are ferromagnetically ordered can be quite large. A system of size $L < R_f$ will always exhibit ferromagnetic order. Thus, it may be difficult to numerically test the Imry-Ma statement that a random field, however weak it may be, destroys the long-range order in three dimensions. Even when R_f is small compared to L it may not be easy to distinguish between spontaneously magnetized states and zero-magnetization states because of the magnetization arising from statistical fluctuations. The problem is similar to that of a finite-size paramagnet: N spins randomly distributed between spin-up and spin-down states will have an average total magnetization proportional to $\sqrt{N}$ and thus average magnetization per spin proportional to $1/\sqrt{N}$.

The magnetization of the system is given by

$$\mathbf{m} = \frac{1}{N} \sum_i \mathbf{s}_i, \tag{1.16}$$

where N is the total number of spins. The absolute value of m is related to the spin correlation function of Eq. (3.5) as

$$m^2 = C(\infty) + \frac{1}{V} \int d^d R \left[C(\mathbf{R}) - C(\infty) \right], \tag{1.17}$$

where $C(\infty)$ describes long-range order (LRO) and $V = L^3$ is the system volume. Plotting m^2 vs $1/V$ shows if there is a LRO in the system in the limit $V \to \infty$.

This means that the systems solved numerically must have a size $L \gg R_f$, must be strongly fulfilled in order to properly make conclusions on the absence of long range order in these systems.

Chapter 2

Topology and random fields

In this chapter, we will focus on the random field model described by the Hamiltonian

$$\mathcal{H} = \int d^d r \left[\frac{\alpha}{2} \left(\boldsymbol{\nabla} \mathbf{S}(\mathbf{r}) \right)^2 - \mathbf{h}(\mathbf{r}) \cdot \mathbf{S}(\mathbf{r}) - \mathbf{H} \cdot \mathbf{S}(\mathbf{r}) \right], \tag{2.1}$$

where $\mathbf{S}(\mathbf{r})$ is an n component continuous symmetry order parameter, $\mathbf{h}(\mathbf{r})$ is an n component random field, and $\mathbf{H}$ is an external field. The random field may be correlated on some scale R_a, in this case,

$$\langle h_\alpha(\mathbf{r}') h_\beta(\mathbf{r}'') \rangle = \frac{1}{n} h^2 a^d \delta_{\alpha\beta} \delta(\mathbf{r}' - \mathbf{r}''), \tag{2.2}$$

where $\Gamma(r)$ rapidly goes to zero at $r \gg R_a$, e.g., $\Gamma(r) = \exp(-r/R_a)$ or $\Gamma(r) = \exp(-r^2/R_a^2)$. The random field may also be uncorrelated, as we will focus on for our numerical computations, in which case $\Gamma(r) = \delta(r)$. This behavior can be generated by drawing realizations of the random field $\mathbf{h}(\mathbf{r})$ from the Gaussian distribution[39],

$$P[\mathbf{h}(\mathbf{r})] \propto \exp\left[-\frac{1}{h^2} \int \frac{d^d r}{a^d} \mathbf{h}^2(\mathbf{r}) \right]. \tag{2.3}$$

This chapter is based on work originally presented in Ref. [38]

In Section 1.1, we presented the argument that the random field $\mathbf{h}(\mathbf{r})$ should destroy long-range order, regardless of its strength. However, we will see here that the actual situation is more complicated and that the long-range behavior of random-field systems is controlled by topology. Our emphasis is on glassy vs reversible behavior. The condition $\mathbf{S}^2 = S_0^2 = \text{const}$ leaves $n-1$ components of the field independent. At $n \leq d$, mapping of $n-1$ independent parameters describing the field $\mathbf{S}$ onto spatial coordinates provides topological defects with singularities. They are vortices in the xy model ($n = 2$) in $2d$, vortex loops in the xy model in $3d$, and hedgehogs in the Heisenberg model ($n = 3$) in $3d$. Energy barriers associated with creation/annihilation of these topological defects and their pinning by the random field make the final state of the system strongly dependent on the initial condition, thus invalidating the Imry-Ma argument. Moreover, as we shall see, the Imry-Ma state necessarily contains singularities that make its energy higher than that of the ordered state.

In the opposite case of $n-1 > d$ a mapping of the $\mathbf{S}$-space onto the $\mathbf{r}$-space that generates topological objects is impossible. In the absence of these topological objects, they do not create energy barriers and cannot be pinned. The stable state of the system is unique and independent of the initial condition. In this case the long-range order is destroyed in a manner that agrees quantitatively with the Imry-Ma picture. This applies to the Heisenberg model with $n = 3$ (and greater) in one dimension, $n = 4$ (and greater) in two dimensions, and $n = 5$ (and greater) in $3d$. The case of $n = d+1$ is the borderline between the above two cases. This corresponds to models with non-singular topological objects: Kinks in the xy model in $1d$, skyrmions in the Heisenberg model with $n = 3$ in $2d$, and similar non-singular solutions for $n = 4$ in $3d$. They are characterized by a topological charge, $Q = \pm 1, \pm 2, ...$ Its conservation is important as it is only weakly violated by the discreteness of the lattice and by a weak random field. Possession of a pinned topological charge by the IM state prevents the system from relaxing to this state from any initial state that has a different topological charge.

To illustrate the validity of the above arguments, we have numerically studied the discrete counterpart of the Hamiltonian (2.1)

$$\mathcal{H} = -\frac{1}{2}\sum_{ij} J_{ij}\mathbf{s}_i \cdot \mathbf{s}_j - \sum_i \mathbf{h}_i \cdot \mathbf{s}_i - \mathbf{H} \cdot \sum_i \mathbf{s}_i, \tag{2.4}$$

on lattices containing hundreds of millions spins $\mathbf{s}_i$ of length s. The relation between parameters of the continuous and discrete models is $\alpha_e = Ja^{d+2}$, $S_0 = s/a^d$, where a is the lattice parameter. We will consider the discrete version of uncorrelated disorder given by $\Gamma(r) = \delta(r)$ in Eq. (2.2),

$$\langle h_{i\alpha} h_{j\beta} \rangle = \frac{h^2}{n}\delta_{\alpha\beta}\delta_{ij}. \tag{2.5}$$

We consider hypercubic lattices with periodic boundary conditions containing L^d spins; L being the linear size of the system. In computations we use $J = s = a = 1$ and $h = H_R$. Our numerical method combines sequential rotations of spins towards the direction of the local effective field, in this case, $\mathbf{H}_{i,\text{eff}} = \sum_i J_{ij}\mathbf{s}_j + \mathbf{h}_j + \mathbf{H}$, with energy-conserving spin flips described by Eq. (1.15) in accordance with the method described in 1.2. Relaxation of the per-site magnetization, $m = \sqrt{\mathbf{m} \cdot \mathbf{m}}$, where $\mathbf{m} = (sN)^{-1}\sum_i \mathbf{S}_i$, out of a collinear state is shown in Fig. 2.1. For each process it was checked that the running time was sufficient to have no further relaxation in the final state.

2.1 Relaxation

In one dimension, numerical analysis of different spin configurations shows that for $n = d + 1 = 2$ the IM-like state with $m = 0$ has the lowest energy. This state, however, cannot be achieved through relaxation from the initially ordered state without forming non-singular kinks or antikinks associated with the full clockwise or counterclockwise rotations of the spin as one moves along the spin chain. While the system tends to disorder it cannot do so

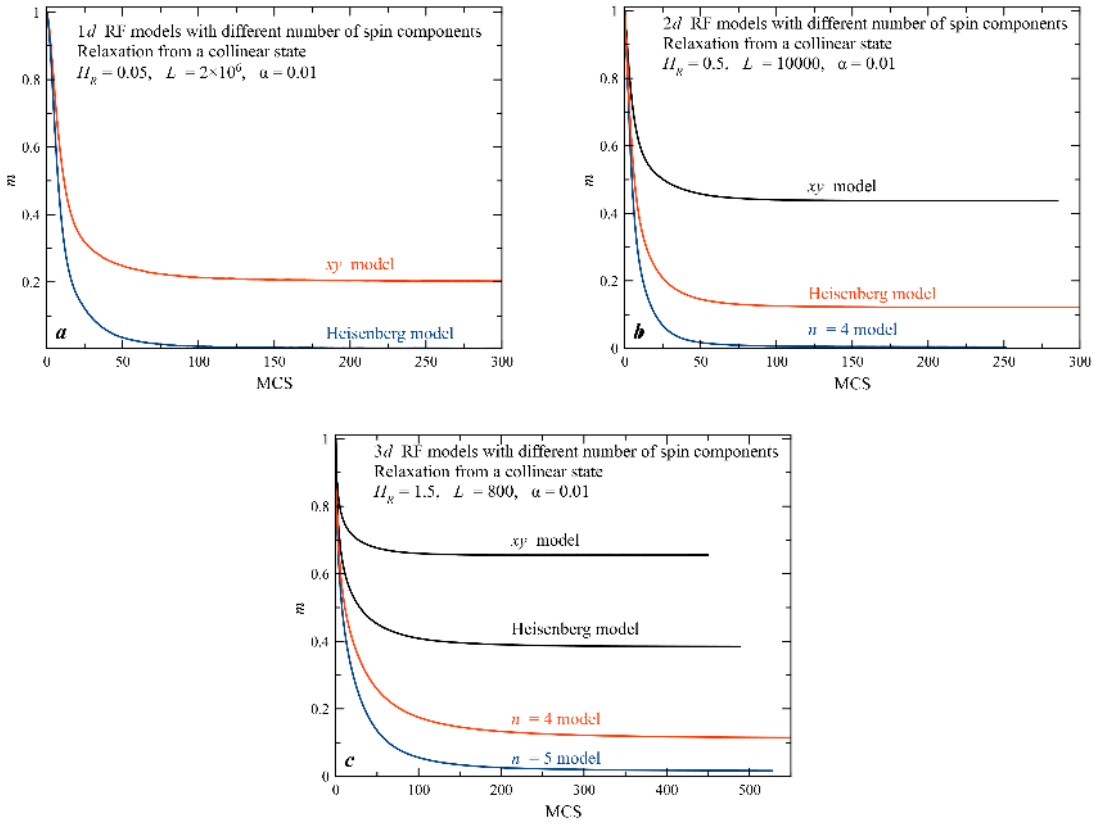

Figure 2.1: Relaxation of the magnetization of the random-field spin system from fully ordered initial state for different d and n: (a) $d = 1$, $n = 2, 3$; (b) $d = 2$, $n = 2, 3, 4$; (c) $d = 3$, $n = 2, 3, 4, 5$. MCS means a full spin update, as in Monte Carlo simulations.

completely because it requires changing the topological charge given by the difference in the number of kinks and antikinks pinned by the random field. However, for three-component spins in one dimension, topologically stable objects are absent and the system disorders completely as is illustrated by Fig. 2.1a.

Two-component spins in two dimensions form well-known topological singularities – vortices in the xy model [35, 40, 41]. Here again the system wants to relax to the IM-like state with $m = 0$ but cannot do it without forming vortices that cost energy, which explains the curve in Fig. 2.1b for the xy model in $2d$. In the marginal case of $d = 2$, $n = 3$ the model possesses non-singular topological objects – skyrmions [40]. In the absence of the random field the difference in the number of skyrmions and antiskyrmions is a conserved topological charge. Skyrmions on the lattice tend to collapse [42]. However, pinning by the random field stabilizes them. We have numerically checked that for $d = 2$, $n = 3$ the IM state with $m = 0$ has the lowest energy. However, conservation of the topological charge prevents the system from relaxing to this state from almost any initial condition. This effect is responsible for a small but finite magnetization obtained by the relaxation from the initially ordered state, see Fig. 2.1b. However, for a four-component spin in two dimensions, topological objects are absent and the system relaxes to the state with $m = 0$, see Fig. 2.1b.

Relaxation in a three-dimensional case is illustrated by Fig. 2.1c. For $n = 2$ the system possesses vortex lines or loops that in the lattice model are singular pancake vortices in $2d$ planes stuck together, see Fig. 2.2a. Similarly, the model with three-component spins in $3d$ has singular hedgehogs, where all spins around a singular point are directed either towards or away from the singularity, see Fig. 2.2b. The energy cost of vortex loops and hedgehogs prevents the $3d$ system of spins from relaxing to the $m = 0$ state, as is shown in Fig. 2.1c. Starting from random orientation of spins one obtains states of vortex or hedgehog glasses with $m = 0$ and energies higher than those of the ordered states. In the marginal case of $n = 4$ the $3d$ random-field model has non-singular topological structures pinned by the

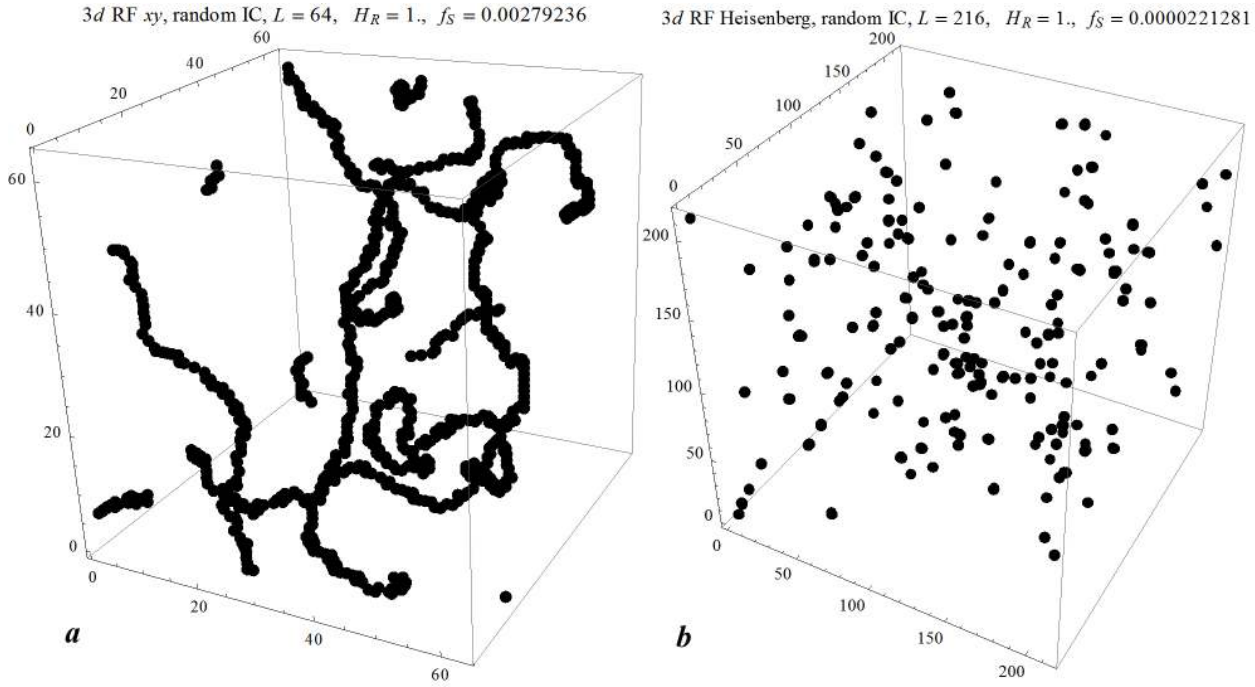

Figure 2.2: Topological simgularities in the random-field spin model in three dimensions obtained by relaxation from random initial orientation of spins: (a) Pinned vortex loops of the xy ($n = 2$) model; (b) Pinned hedgehogs of the Heisenberg ($n = 3$) model. f_S is fraction of the lattice interstitial (body centered) sites occupied by singularities.

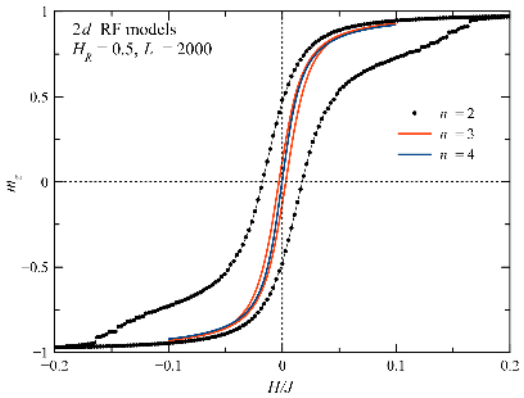

Figure 2.3: Hysteresis curves of the random field spin model in two dimensions for $n = 2, 3, 4$.

random field which are similar to skyrmions in $2d$. In this case the final magnetic moment is still non-zero but small, see Fig. 2.1c. We again find that the energy of the Imry-Ma-like state $m = 0$ state for $d = 3$, $n = 4$ is lower than that of the $m \neq 0$ state. However, the difference in the topological charge prevents the system from relaxing to the Imry-Ma state from almost any initial state.

The model with five-component spins in $3d$ does not possess any topologically stable structures. The relaxation of the system from the ordered initial state is unobstructed by any topological arguments and the system ends up in the state with $m = 0$, Fig. 2.1c.

2.2 Hysteresis

The relation between topology and metastability in, e.g., two spatial dimensions is further illustrated by the hysteresis curves in Fig. 2.3. The model with $n = 2$, that possesses xy vortices with singularities, is characterized by a sizable hysteresis loop which is indicative of strong metastability. The loop becomes thin for $n = 3$ when non-singular skyrmions are present. It disappears completely, resulting in a reversible magnetic behavior, at $n = 4$ when topological objects are absent. Similar behavior for different n has been observed in $3d$.

2.3 Defects in the Imry-Ma Picture

Applying the Imry-Ma argument given in Section 1.1, Eq. (1.9) becomes $R_f \propto (Js/h)^{2/(4-d)}$. For $R \gtrsim R_f$ correlations should be completely destroyed, thus the state of the system should be disordered. This famous argument, however, does not account for the energy associated with unavoidable singularities at $n \leq d$. To show their existence in the IM state, consider components of the averaged random field $\bar{h}_\beta$, $\beta = 1, \ldots, n$. Since $\bar{h}_\beta$ are sums of many random numbers, they are statistically independent and have Gaussian distribution. In about a half of the space $\bar{h}_\beta > 0$, in the other half $\bar{h}_\beta < 0$. Boundaries between these regions are subspaces of dimension $d-1$, where $\bar{h}_\beta = 0$. Their intersection, that is, $\bar{\mathbf{h}} = 0$, is unavoidable and forms a subspace of dimension $d-n$ if $n \leq d$. It is easy to see that subspaces with $\bar{\mathbf{h}} = 0$ are singularities in the spin field $\mathbf{S}$. Since $\mathbf{S}^2 = \text{const}$, crossing subspaces $\bar{\mathbf{h}} = 0$ makes all components of $\mathbf{S}$ change direction. For $n = 2$ in $2d$ subspaces $\bar{\mathbf{h}} = 0$ are points and the corresponding singularities are vortices or antivortices. A spin field in the $2d$ xy model generated in accordance with the IM prescription is shown in Fig. 2.4. The red line corresponds to $\bar{h}_x = 0$ and thus spins directed along the y-axis. The blue line corresponds to $\bar{h}_y = 0$ and thus spins directed along the x-axis. At the intersections of red and blue lines the spins can look neither in the x nor in the y-direction. This generates topological defects – vortices or antivortices. For $n = 2$ in $3d$ subspaces $\bar{\mathbf{h}} = 0$ are lines and the singularities are vortex lines or loops. For $n = 3$ in $3d$ subspaces $\bar{\mathbf{h}} = 0$ are points and the singularities are hedgehogs. They emerge at the intersection of surfaces corresponding to $\bar{h}_x = 0$, $\bar{h}_x = 0$, and $\bar{h}_x = 0$, see Fig. 2.5.

By order of magnitude the number of singularities equals the number of IM domains, $(L/R_f)^d$. The lowest energy of an xy vortex in a $2d$ IM state would be $2\pi J s^2 \ln(R_f/a)$[40]. The energy of the vortex loop in $3d$ contains an additional factor R_f/a. Consequently, the exchange energy per spin goes up by $\ln(R_f/a)$ as compared to the IM argument that

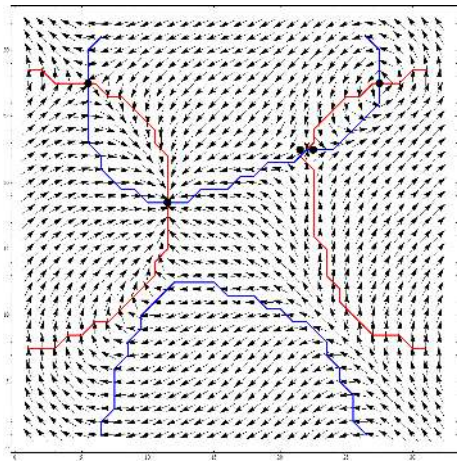

Figure 2.4: Emergence of vortices and antivortices at the intersections of lines corresponding to $\bar{h}_x = 0$ (red) and $\bar{h}_y = 0$ (blue) in the random-field $2d$ xy model. Picture reflects numerical averaging of $\mathbf{h}$ within finite range according to the prescription of the Imry-Ma model for a particular realization of the random field. Arrows show spins on lattice sites. Similar structures emerge after relaxation from random orientation of spins, with the positions of vortices depending on the initial state.

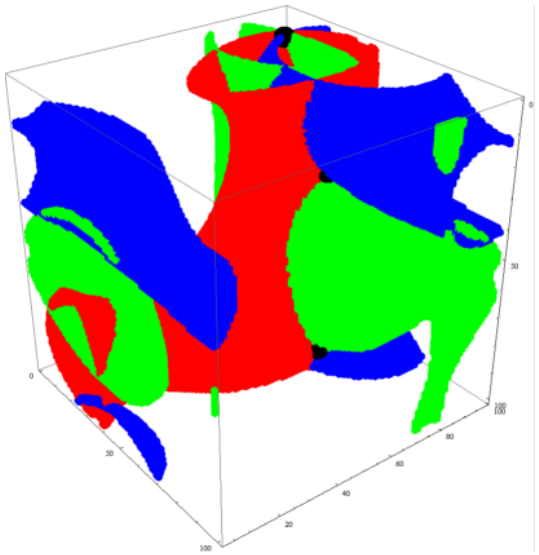

Figure 2.5: Emergence of hedgehogs (black) at the intersection of three surfaces (shown in different color) corresponding to $\bar{h}_x = 0$, $\bar{h}_y = 0$, and $\bar{h}_z = 0$ respectively in the $n = 3$ random-field model in three dimensions.

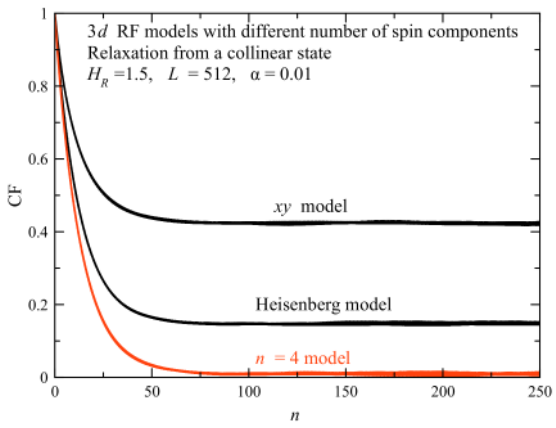

Figure 2.6: Spin-spin correlation function of the random-field model for $n = 2, 3, 4$ in three dimensions.

neglects vortices. The energy of a hedgehog would be $4\pi Js^2(R_f/a)$. It changes the exchange energy by a numerical factor of order unity. Thus, topological defects only modify the IM argument by making R_f go up logarithmically in the xy model and by a factor of order unity in the Heisenberg model. However, the energies of topological defects that are needed to form the IM state as the system disorders are high compared to the Curie temperature. This prohibits relaxation to $m = 0$ even at elevated temperatures. However, for the case of $n > d$, the averaged random field is non-zero everywhere and the spin field $\mathbf{S}$ is non-singular. Still at $n = d+1$ the presence of non-singular topological objects and conservation of topological charge prevents the ordered state from relaxing to the IM state. However, for $n > d$, the averaged random field is non-zero everywhere and the spin field $\mathbf{S}$ is non-singular. Consequently, at $n > d$ the $m = 0$ state has the lowest energy in accordance with the Imry-Ma argument and the Aizenman-Wehr theorem which assume continuity of the spin field[3, 43]. Still at $n = d + 1$ the presence of non-singular topological objects and conservation of topological charge prevents the ordered state from relaxing to the $m = 0$ Imry-Ma state. Only at $n > d + 1$, when the spin-field is continuous and topological objects are absent the system relaxes to the Imry-Ma state.

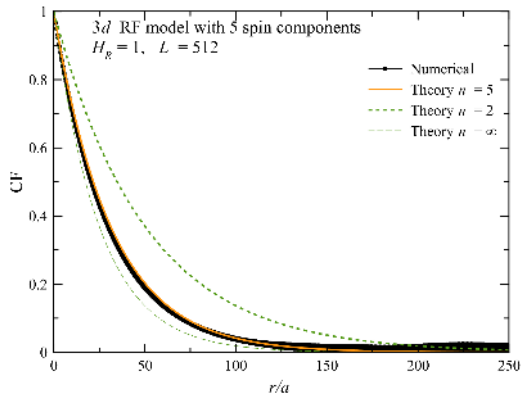

Figure 2.7: Theoretical (see text) and numerical spin-spin correlation functions of the $3d$ random-field model at $n = 5$.

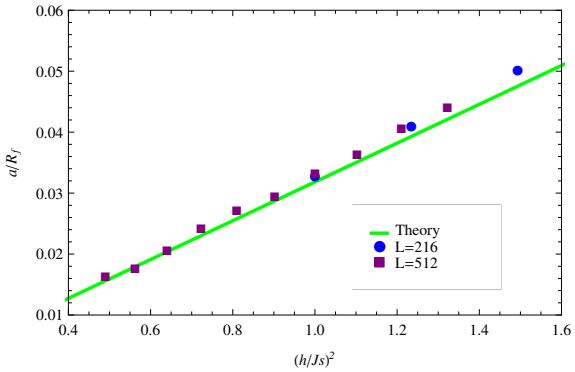

Figure 2.8: Dependence of R_f on h computed numerically (points) for the $n = 5$ random-field model in three dimensions and given by Eq. (2.16) (solid line) at $n = 5$.

2.4 Correlation Functions

We have computed spin-spin correlation functions in the final state obtained through relaxation from the initially ordered state. Fig. 2.6 shows the $3d$ spin-spin correlation function for $n = 2, 3, 4$. At $n \leq d + 1$ and $R_f \ll L$ the ferromagnetic order persists: The correlation function at large distances falls to a plateau that coincides with m^2 of the plateau in Fig. 2.1. Meanwhile, at $n > d+1$ the order is fully destroyed in accordance with the IM picture. The $3d$ correlation function for $n = 5$ is shown in Fig. 2.7.

In 3d, we can enforce the constraint that $\mathbf{S}^2 = S_\circ^2 = \text{const.}$ by adding a Lagrange

multiplier term to the Hamiltonian

$$\mathcal{H}_\lambda = \mathcal{H} - \int d^3r\, \lambda(\mathbf{r})\mathbf{S}^2. \tag{2.6}$$

The extremal configurations of this Hamiltonian give

$$\alpha\nabla^2\mathbf{S} + \mathbf{h} + 2\lambda\mathbf{S} = 0. \tag{2.7}$$

Multiplying by $\mathbf{S}$, we find

$$\lambda = -\frac{1}{2S_\circ^2}\left(\alpha\mathbf{S}\cdot\nabla^2\mathbf{S} + \mathbf{S}\cdot\mathbf{h}\right) \tag{2.8}$$

$$\alpha\nabla^2\mathbf{S} - \frac{\alpha}{S_\circ^2}\mathbf{S}(\mathbf{S}\cdot\nabla^2\mathbf{S}) + \mathbf{h} - \frac{1}{S_\circ^2}\mathbf{S}(\mathbf{S}\cdot\mathbf{h}) = 0 \tag{2.9}$$

In the second term of Eq. (2.9)

$$\mathbf{S}\cdot\nabla^2\mathbf{S} = \partial_u(\mathbf{S}\cdot\partial_u\mathbf{S}) - \partial_u\mathbf{S}\cdot\partial_u\mathbf{S} = -\partial_u\mathbf{S}\cdot\partial_u\mathbf{S} \tag{2.10}$$

as

$$\mathbf{S}\cdot\partial_u\mathbf{S} = \frac{1}{2}\partial_u\mathbf{S}^2 = 0 \tag{2.11}$$

At small volumes, $\mathbf{S}$ is approximately aligned. This term is quadratic in the small change in alignment, while the other terms are only linear, so it can safely be ignored. The solution to the remaining equation is given by Green's theorem as

$$\mathbf{S}(\mathbf{r}) = -\frac{1}{\alpha}\int d^3r'\, G(\mathbf{r}-\mathbf{r}')\left[\mathbf{h}(\mathbf{r}') - \frac{\mathbf{S}(\mathbf{r}')\left(\mathbf{S}(\mathbf{r}')\cdot\mathbf{h}(\mathbf{r}')\right)}{S_\circ^2}\right] \tag{2.12}$$

with $G(\mathbf{r}) = -1/4\pi|\mathbf{r}|$ the Green function of the Laplace equation in 3d. Then

$$\frac{1}{2S_\circ^2}\langle[\mathbf{S}(\mathbf{r}_1)-\mathbf{S}(\mathbf{r}_2)]^2\rangle = \frac{1}{2\alpha^2 S_\circ^2}\int d^3r' \int d^3r''\,[G(\mathbf{r}_1-\mathbf{r}')-G(\mathbf{r}_2-\mathbf{r}')]\,[G(\mathbf{r}_1-\mathbf{r}'')-G(\mathbf{r}_2-\mathbf{r}'')]\,\langle \mathbf{q}(\mathbf{r}')\cdot\mathbf{q}(\mathbf{r}'')\rangle, \tag{2.13}$$

where $\mathbf{g} \equiv \mathbf{h} - \mathbf{S}(\mathbf{S}\cdot\mathbf{h})/S_\circ^2$.

Assuming that there is no correlation between $\mathbf{h}$ and $\mathbf{S}$ and using the uncorrelated version of Eq. (2.2), we find

$$\langle \mathbf{q}(\mathbf{r}')\cdot\mathbf{q}(\mathbf{r}'')\rangle = \frac{h^2}{n}(n-1)a^3\delta(\mathbf{r}'-\mathbf{r}'') \tag{2.14}$$

and

$$\frac{1}{2S_\circ^2}\langle[\mathbf{S}(\mathbf{r}_1)-\mathbf{S}(\mathbf{r}_2)]^2\rangle = \frac{h^2a^3}{2\alpha^2 S_\circ^2}\left(1-\frac{1}{n}\right)\int d^3r\,[G(\mathbf{r}_1-\mathbf{r})-G(\mathbf{r}_2-\mathbf{r})]^2 = \frac{|\mathbf{r}_1-\mathbf{r}_2|}{R_f} \tag{2.15}$$

with

$$\frac{R_f}{a} = \frac{8\pi}{1-1/n}\cdot\left(\frac{\alpha S_\circ}{ha^2}\right)^2. \tag{2.16}$$

This gives a general form for the short distance correlation function in 3d as

$$\langle \mathbf{S}(\mathbf{r}_1)\cdot\mathbf{S}(\mathbf{r}_2)\rangle = S_\circ^2\left(1-\frac{|\mathbf{r}_1-\mathbf{r}_2|}{R_f}\right) \tag{2.17}$$

This short-range form of the correlation function agrees with our numerical results for all n in $3d$. For $n \geq 5$ the spin-spin correlation function at all distances can be very well fitted by $\langle \mathbf{s}(\mathbf{r}_1)\cdot\mathbf{s}(\mathbf{r}_2)\rangle = \exp(-|\mathbf{r}_1-\mathbf{r}_2|/R_f)$. The good agreement with this formula is illustrated by Fig. 2.7. So far we have been able to prove analytically the numerically confirmed

exponential decay of the correlation function in $3d$ only for the mean-spherical model which corresponds to $n = \infty$ [44]. However, the observed exponential behavior of $\langle \mathbf{s}(\mathbf{r}_1) \cdot \mathbf{s}(\mathbf{r}_2) \rangle$ and the observed $1/h^2$ dependence of R_f on the strength of the random field for small h at $n = 5, d = 3$ (see Fig. 2.8) present clear evidence of the onset of the Imry-Ma state in the absence of topological objects.

2.5 Discussion

We have demonstrated that topology of the order parameter controls whether the random-field system exhibits reversible or irreversible behavior. For the n-component spin in d dimensions the presence of topological structures at $n \leq d+1$ gives rise to vortex, hedgehog, and skyrmion glasses. These structures can be pinned by the random field, creating metastability. Furthermore, the Imry-Ma state requires the creation of defects, which increases its energy.

Meanwhile, for $n > d + 1$, when topological structures are absent, the behavior of the system is reversible and spin-spin correlations agree quantitatively with the Imry-Ma picture. These findings provide the guiding principle for assessing the long-range behavior of various systems with quenched randomness and continuous-symmetry order parameter, which we will use in our studies of various systems in the following chapters.

Chapter 3

Random field XY model in three dimensions

In this chapter, we will build on the understanding gained in the previous chapter on random fields, focusing on the case of $n = 2$, $d = 3$, otherwise known as the XY model in 3d.

This model is especially convenient for doing analytic calculations, as the configuration of the order parameter at a given point in space can be described using a single angle. Writing

$$\mathbf{s}(\mathbf{r}) = s[\sin\phi(\mathbf{r}), \cos\phi(\mathbf{r})] \tag{3.1}$$

$$\mathbf{h}(\mathbf{r}) = h[\sin\varphi(\mathbf{r}), \cos\varphi(\mathbf{r})] \tag{3.2}$$

and assuming that $\mathbf{H}$ is directed along the x axis, $\mathbf{H} = (H, 0)$, one obtains from Eq. (2.1)

$$\mathcal{H} = s \int \frac{d^d r}{a^d} \left[\frac{Jsa^2}{2} (\nabla\phi)^2 - h\cos(\phi - \varphi) - H\cos\phi \right]. \tag{3.3}$$

This chapter is based on work originally presented in Ref. [41] and Ref. [45]

Thus we can re-write the Hamiltonian of Eq. (2.4) as

$$\mathcal{H} = \frac{Js^2}{2} \sum_{ij} \cos(\phi_i - \phi_j) - hs \sum_i \cos(\theta_i - \phi_j) - H \sum_i \cos\phi_i \tag{3.4}$$

where ϕ is the angle of our order parameter and φ is the angle of the random field. We will calculate analytically and numerically the correlation function (CF) defined by

$$C(R) = \frac{1}{N} \sum_i \langle \mathbf{s}(\mathbf{r}_i) \cdot \mathbf{s}(\mathbf{r}_i + \mathbf{R}) \rangle \,, \tag{3.5}$$

where N is the total number of spins. In analytical calculations, there is no averaging over i and $\langle \ldots \rangle$ mean averaging over realizations of the random field. In numerical work, $\langle \ldots \rangle$ can be dropped for large enough system sizes where there is a sufficient self-averaging.

3.0.1 Energy scaling

Writing out Eq. (1.9) in terms of the Hamiltonian Eq. (3.3),

$$R_f \sim a \left(\frac{sJ}{h} \right)^{2/(4-d)} . \tag{3.6}$$

Finiteness of R_f for any $d < 4$ supports the initial assumption that spins follow the averaged RF and thus the state is disordered, $m = 0$. The resulting energy of the IM state is

$$E - E_0 \sim -s^2 J \left(\frac{h}{sJ} \right)^{4/(4-d)} \tag{3.7}$$

that yields $E - E_0 \sim -h^4/J^3$ in $3d$. However, the main contribution to the adjustment energy arizes at the atomic scale and is given by $E - E_0 \sim -h^2/J$ in all dimensions.

One can modify the IM argument by taking into account adjustment of spins to the RF at all length scales. For this purpose, consider a reference state perfectly ordered in some

direction. Spins will turn away from this state under the influence of the RF. More precisely, groups of spins of linear size R will rotate by an adjustment angle ϕ (considered as small to begin with) under the influence of the RF averaged over this region. The corresponding energy per spin is given by the equation

$$E - E_0 \sim -sh \left(\frac{a}{R}\right)^{d/2} \phi + s^2 J \left(\frac{a}{R}\right)^2 \phi^2. \tag{3.8}$$

Minimizing this expression with respect to ϕ, one obtains

$$\phi \sim \frac{h}{sJ} \left(\frac{R}{a}\right)^{(4-d)/2} \tag{3.9}$$

that grows with the distance R, as expected. The square of the angular deviation increases as $\phi^2 \sim (R/R_f)^{4-d}$, where R_f is given by Eq. (3.6). This defines the spin CF at small distances

$$C(R) = s^2 \cos\phi \cong s^2 \left(1 - \frac{1}{2}\phi^2\right) = s^2 \left[1 - A \left(\frac{R}{R_f}\right)^{4-d}\right], \tag{3.10}$$

where A is a number.

The energy per spin corresponding to spin adjustment at the distance R is

$$E - E_0 \sim -\frac{h^2}{J} \left(\frac{a}{R}\right)^{d-2}. \tag{3.11}$$

One can see that the highest energy gain is provided by spin adjustments at the atomic scale, $R \sim a$. In this case one obtains

$$E - E_0 \sim -h^2/J. \tag{3.12}$$

Spin misalignments grow large, $\phi \sim 1$, at $R \sim R_f$. Substituting R_f into Eq. (3.11), one recovers the IM energy of Eq. (3.7). It should be stressed that the IM energy is much smaller than the main short-distance energy contribution and it is not accessible numerically.

It has been speculated [46] that at $R > R_f$, when ϕ becomes large, it is distributed with a Gaussian probability, making the energy associated with the random field scale as $sh(a/R)^{d/2}\exp(-\phi^2/2)$ instead of $-sh(a/R)^{d/2}\phi$ for small ϕ. Then the minimum of the total energy that includes the exchange energy $s^2J(a/R)^2\phi^2$, would correspond to $\phi^2 \sim (4-d)\ln(R/R_f)$ in accordance with the Bragg glass result. [13, 29, 30]

3.1 Analytical results

If the random field is sufficiently strong, then in the absence of a strong external field, a strong local Zeeman interaction should align the spins with the random field at each site independently. The case of a weak random field is less straightforward. On one hand, such a field cannot destroy the parallel alignment of neighboring spins created by the strong ferromagnetic exchange. On the other hand, neither the exchange nor the local random field can determine the direction of the local magnetization. The latter can, therefore, wander around the sample, with some characteristic ferromagnetic correlation length that can be, in principle, either finite or infinite. This non-obvious effect of the weak random field will be the main focus of our investigation.

3.1.1 Angular correlations

At $H = 0$ the correlation function of the spin angles ϕ can be computed by noticing that the extremal configurations of $\phi(\mathbf{r})$ with the Hamiltonian (3.3) satisfy

$$Jsa^2\nabla^2\phi = h\sin(\phi-\varphi) = h_x\sin\phi - h_y\cos\phi \tag{3.13}$$

where $h_x = h\cos\varphi$ and $h_y = h\sin\varphi$. This equation has an implicit solution

$$\phi(\mathbf{r}) = \frac{1}{Jsa^2}\int d^dr' G_d(\mathbf{r}-\mathbf{r}') \times [h_x(\mathbf{r}')\sin\phi(\mathbf{r}') - h_y(\mathbf{r}')\cos\phi(\mathbf{r}')], \tag{3.14}$$

where $G_d(\mathbf{r})$ is the Green function of the Laplace equation in d dimensions: $G_2(\mathbf{r}) = -(2\pi)^{-1}\ln|\mathbf{r}|$ and $G_3(\mathbf{r}) = -1/(4\pi|\mathbf{r}|)$. Its Fourier transform is $G_d(\mathbf{q}) = -1/\mathbf{q}^2$ for all d. Eq. (3.14) then gives

$$\begin{aligned}
&\langle[\phi(\mathbf{r}_1)-\phi(\mathbf{r}_2)]^2\rangle = \frac{1}{J^2s^2a^4}\int d^dr'\int d^dr'' \times \\
&[G_d(\mathbf{r}_1-\mathbf{r}') - G_d(\mathbf{r}_2-\mathbf{r}')][G_d(\mathbf{r}_1-\mathbf{r}'') - G_d(\mathbf{r}_2-\mathbf{r}'')] \\
&\times[\langle h_x(\mathbf{r}')h_x(\mathbf{r}'')\rangle\langle\sin\phi(\mathbf{r}')\sin\phi(\mathbf{r}'')\rangle \\
&+\langle h_y(\mathbf{r}')h_y(\mathbf{r}'')\rangle\langle\cos\phi(\mathbf{r}')\cos\phi(\mathbf{r}'')\rangle \\
&-\langle h_x(\mathbf{r}')h_y(\mathbf{r}'')\rangle\langle\sin\phi(\mathbf{r}')\cos\phi(\mathbf{r}'')\rangle \\
&-\langle h_y(\mathbf{r}')h_x(\mathbf{r}'')\rangle\langle\cos\phi(\mathbf{r}')\sin\phi(\mathbf{r}'')\rangle]
\end{aligned} \tag{3.15}$$

Here we used the fact that for a weak random field the direction of the spin at a particular site must have very weak correlation with the direction of the random field at that site, leading to $\langle h_x(\mathbf{r}')h_x(\mathbf{r}'')\sin\phi(\mathbf{r}')\sin\phi(\mathbf{r}'')\rangle \approx \langle h_x(\mathbf{r}')h_x(\mathbf{r}'')\rangle\langle\sin\phi(\mathbf{r}')\sin\phi(\mathbf{r}'')\rangle$ and so on.

With the help of Eq. (2.2), one obtains in three dimensions at $H = 0$

$$\begin{aligned}
&\langle[\phi(\mathbf{r}_1)-\phi(\mathbf{r}_2)]^2\rangle = \\
&\frac{h^2}{2J^2s^2a}\int d^3r[G_3(\mathbf{r}_1-\mathbf{r}) - G_3(\mathbf{r}_2-\mathbf{r})]^2 = \\
&\frac{h^2}{J^2s^2a}\int\frac{d^3q}{(2\pi)^3}\frac{1-\cos[\mathbf{q}\cdot(\mathbf{r}_1-\mathbf{r}_2)]}{q^4} = \\
&\frac{h^2}{8\pi J^2s^2a}|\mathbf{r}_1-\mathbf{r}_2|
\end{aligned} \tag{3.16}$$

and, finally,

$$\langle[\phi(\mathbf{r}_1)-\phi(\mathbf{r}_2)]^2\rangle = 2\frac{|\mathbf{r}_1-\mathbf{r}_2|}{R_f}, \qquad \frac{R_f}{a} = 16\pi\left(\frac{Js}{h}\right)^2, \tag{3.17}$$

where R_f is the ferromagnetic correlation length. As we shall see later, this formula is in excellent agreement with numerical results. The linear decay of short-range correlations due to the random field was first obtained by Larkin in the application to translational correlations in flux lattices. [1] Extrapolating Eq. (3.17) to greater distances, one should expect that the spin field would rotate significantly at distances $|\mathbf{r}_1-\mathbf{r}_2| \sim R_f$. The long-range behavior of spin-spin correlations has been, however, subject of a significant controversy in the last forty years.

3.1.2 Spin correlations

At short distances the spin correlation function directly follows from the angular-deviation correlator computed above:

$$\begin{aligned}\langle \mathbf{s}(\mathbf{r}_1)\cdot\mathbf{s}(\mathbf{r}_2)\rangle &= s^2\langle\cos[\phi(\mathbf{r}_1)-\phi(\mathbf{r}_2)]\rangle \\ &= s^2\left(1-\frac{1}{2}\langle[\phi(\mathbf{r}_1)-\phi(\mathbf{r}_2)]^2\rangle\right) \\ &= s^2\left(1-\frac{|\mathbf{r}_1-\mathbf{r}_2|}{R_f}\right),\end{aligned} \tag{3.18}$$

in accordance with Eq. (3.10) in $3d$. More generally, one can write

$$\begin{aligned}&\langle \mathbf{s}(\mathbf{r}_1)\cdot\mathbf{s}(\mathbf{r}_2)\rangle = s^2\langle\cos[\phi(\mathbf{r}_1)-\phi(\mathbf{r}_2)]\rangle \\ &= s^2\exp\left\{-\frac{1}{2}\langle[\phi(\mathbf{r}_1)-\phi(\mathbf{r}_2)]^2\rangle\right\}.\end{aligned} \tag{3.19}$$

Substituting here Eq. (3.17), in $3d$ one obtains

$$\langle \mathbf{s}(\mathbf{r}_1) \cdot \mathbf{s}(\mathbf{r}_2) \rangle = s^2 \exp\left(-\frac{|\mathbf{r}_1 - \mathbf{r}_2|}{R_f} \right). \tag{3.20}$$

Equation (3.20) can be obtained in the whole range of distances by the functional integration over the distribution of the random field given by Eq. (2.3). The calculation in $3d$ proceeds as follows

$$\begin{aligned}
&\langle \mathbf{s}(\mathbf{r}_1) \cdot \mathbf{s}(\mathbf{r}_2) \rangle = s^2 \langle \exp i[\phi(\mathbf{r}_1) - \phi(\mathbf{r}_2)] \rangle \\
&= s^2 \left[\int D\{h_x\} D\{h_y\} \exp\left\{ -\frac{\int d^3r \, (h_x^2 + h_y^2)}{h^2 a^3} \right\} \right]^{-1} \\
&\times \int D\{h_x\} D\{h_y\} \exp\left\{ i \int d^3r [\frac{1}{Jsa^2} [G_3(\mathbf{r} - \mathbf{r}_1) - \right. \\
&\left. G_3(\mathbf{r} - \mathbf{r}_2)][h_x \sin\phi(\mathbf{r}) - h_y \cos\phi(\mathbf{r})] - \frac{h_x^2 + h_y^2}{h^2 a^3}] \right\} \\
&= s^2 \exp\left\{ -\frac{h^2}{4J^2 s^2 a} \int d^3r \, [G_3(\mathbf{r} - \mathbf{r}_1) - G_3(\mathbf{r} - \mathbf{r}_2)]^2 \right\} \\
&= s^2 \exp\left\{ -\frac{h^2}{2J^2 s^2 a} \int \frac{d^3q}{(2\pi)^3} \frac{1 - \cos[\mathbf{q} \cdot (\mathbf{r}_1 - \mathbf{r}_2)]}{q^4} \right\} \\
&= s^2 \exp\left(-\frac{|\mathbf{r}_1 - \mathbf{r}_2|}{R_f} \right),
\end{aligned} \tag{3.21}$$

where we have used Eq. (3.14).

The increase of spin misalignments with distance according to Eq. (3.17) is unquestionable and it is also true that at some distance misalignments become large. It was questioned by many researchers, however, whether the averaging employed to obtain Eq. (3.21) provides correct description of the behavior at large distances. Theory based upon scaling and replica-symmetry breaking arguments [13, 30] yielded $\langle [\phi(\mathbf{r}_1) - \phi(\mathbf{r}_2)]^2 \rangle = A \ln |\mathbf{r}_1 - \mathbf{r}_2|$ at $R \gg R_f$, with A depending on the dimensionality only. While this theory was initially developed for flux lattices, it was later argued that the result must be relevant for the xy random-field spin model as well. [34, 47–49] This would imply universal power law decay of

long-range correlations,

$$\langle \mathbf{s}(\mathbf{r}_1) \cdot \mathbf{s}(\mathbf{r}_2) \rangle \sim \frac{1}{|\mathbf{r}_1 - \mathbf{r}_2|} \tag{3.22}$$

in $3d$ according to Eq. (3.20). Such a quasiordered phase, presumed to be vortex-free in spin systems and dislocation-free in flux lattices, received the name of Bragg glass. As we shall see below neither Imry-Ma argument nor the Bragg glass argument provides the correct description of the random-field system that would agree with numerical results. Crucial for its behavior is magnetic hysteresis, which implies that energy barriers and metastable states play an important role regardless of the strength of the random field. We shall also demonstrate that the behavior of the random-field system cannot be understood without invoking topological defects.

3.1.3 Short-range energy due to random field

The random field contributes to the energy of the system through Zeeman interaction with the spin field and through the exchange energy associated with the non-uniformity of the spin field. The latter can be computed as

$$\langle \mathcal{H}_{\rm ex} \rangle = \frac{1}{2} J \sum_{ij} \langle s^2 - \mathbf{s}_i \cdot \mathbf{s}_j \rangle = \frac{1}{4} J s^2 \sum_{ij} \langle (\phi_i - \phi_j)^2 \rangle, \tag{3.23}$$

where the summation is over N sites i and the nearest neighbors j of each i-site, with six such neighbors in a $3d$ cubic lattice, separated by $|\mathbf{r}_i - \mathbf{r}_j| = a$. According to Eq. (3.17), for the nearest neighbors $\langle (\phi_i - \phi_j)^2 \rangle = h^2/(8\pi J^2 s^2)$, so that per spin

$$\frac{\langle \mathcal{H}_{\rm ex} \rangle}{N} = \frac{1}{4} J s^2 6 \frac{h^2}{8\pi J^2 s^2} = \frac{3h^2}{16\pi J}. \tag{3.24}$$

The total energy is a sum of the exchange energy and Zeeman energy, given by Eq. (2.1). Let us consider the case of $H = 0$. The contribution of the weak random field to the energy

is a sum of almost independent contributions from small volumes inside which the deviation, $\delta\phi(\mathbf{r})$, from the local ferromagnetic alignment of spins is small. Thus, to obtain the main part of the energy due to random field, one can replace ϕ in Eq. (2.1) with $\delta\phi(\mathbf{r}) \ll 1$,

$$\mathcal{H}_{\rm SR} = s \int \frac{d^3r}{a^3} \left[\frac{1}{2} Jsa^2 (\nabla\delta\phi)^2 - h\delta\phi \sin\varphi \right]. \tag{3.25}$$

Low temperature behavior is dominated by the extremal configurations satisfying

$$Jsa^2 \nabla^2 \delta\phi = -h \sin\varphi \tag{3.26}$$

Substituting $\sin\varphi$ from this equation into Eq. (3.25) and integrating by parts one obtains

$$\begin{aligned} \mathcal{H}_{\rm SR} &= s \int \frac{d^3r}{a^3} \left\{ \frac{1}{2} Jsa^2 (\nabla\delta\phi)^2 + Jsa^2 \delta\phi \nabla^2 \phi \right\} \\ &= s \int \frac{d^3r}{a^3} \left\{ \frac{1}{2} Jsa^2 (\nabla\delta\phi)^2 - Jsa^2 (\nabla\delta\phi)^2 \right\}. \end{aligned} \tag{3.27}$$

It is clear from this expression that the short-range Zeeman energy is twice the short-range exchange energy with a minus sign,

$$\frac{\langle \mathcal{H}_Z \rangle}{N} = -2 \frac{\langle \mathcal{H}_{\rm ex} \rangle}{N} = -\frac{3h^2}{8\pi J}. \tag{3.28}$$

The total short-range energy per spin is

$$\frac{\langle \mathcal{H} \rangle}{N} = \frac{\langle \mathcal{H}_{\rm ex} \rangle + \langle \mathcal{H}_Z \rangle}{N} = -\frac{3h^2}{16\pi J}, \tag{3.29}$$

in accordance with Eq. (3.12). It is insensitive to the long-range behavior of the spin field, that is, to the spatial scale of the rotation of the direction of the local magnetization over the sample. This is because for a weak random field such rotations involve large distances,

and therefore they contribute much less to the exchange energy then the weak misalignment of the neighboring spins due to the random field. As we shall see below, equations (3.24), (3.28), and (3.29) are in excellent agreement with numerical results. Small deviations are due to the contribution of vortices to the short-range behavior.

3.1.4 Approach to saturation

In the presence of the external magnetic field the extremal configurations satisfy

$$Jsa^2\nabla^2\phi - H\sin\phi = h\sin(\phi-\varphi). \tag{3.30}$$

Let the field H be sufficiently large to ensure a small deviation of spins from the x axis, that is, small angle $\phi(\mathbf{r})$. Then Eq. (3.30) can be approximately written as

$$\nabla^2\phi - k_H^2\phi = -\frac{h}{Jsa^2}\sin\varphi, \tag{3.31}$$

where

$$\frac{1}{k_H^2} = R_H^2 = \left(\frac{Js}{H}\right)a^2. \tag{3.32}$$

The solution of Eq. (3.31) is

$$\phi(\mathbf{r}) = \frac{h}{Jsa^2}\int d^3r' \frac{e^{-k_H|\mathbf{r}-\mathbf{r}'|)}}{4\pi|\mathbf{r}-\mathbf{r}'|}\sin\varphi(\mathbf{r}'). \tag{3.33}$$

Consequently,

$$\langle\phi^2\rangle = \left(\frac{h}{Jsa^2}\right)^2\int d^3r'\int d^3r''\frac{e^{-k_H|\mathbf{r}-\mathbf{r}'|}e^{-k_H|\mathbf{r}-\mathbf{r}''|}}{16\pi^2|\mathbf{r}-\mathbf{r}'||\mathbf{r}-\mathbf{r}''|}\times\langle\sin\varphi(\mathbf{r}')\sin\varphi(\mathbf{r}'')\rangle. \tag{3.34}$$

With the help of Eq. (2.2) one obtains for $k_H a \ll 1$ ($R_H \gg a$)

$$\begin{aligned}\langle\phi^2\rangle =& \frac{a^3}{32\pi^2}\left(\frac{h}{Jsa^2}\right)^2 \int d^3r \frac{e^{-2k_H r}}{r^2} \\ =& \frac{1}{16\pi}\left(\frac{h}{Js}\right)^{3/2}\left(\frac{h}{H}\right)^{1/2}.\end{aligned} \tag{3.35}$$

The above formulas describe the approach to saturation on increasing the field:

$$1-\frac{m}{s} = \langle 1-\cos\phi\rangle = \frac{1}{2}\langle\phi^2\rangle = \frac{1}{32\pi}\left(\frac{h}{Js}\right)^{3/2}\left(\frac{h}{H}\right)^{1/2} \tag{3.36}$$

The square root dependence on H, Eq. (3.36), must hold as long as the field satisfies $R_H > a$, which translates into $H < Js$. At $H > Js$ the length R_H becomes small compared to a and the exchange-generated Laplacian in Eq. (3.31) is no longer relevant because the r in the Green function of that equation cannot be smaller than a. In this case the approach to saturation is dominated by the spin torque of the external field H against the local field $h(\mathbf{r})$. The Laplacian in Eq. (3.31) can be safely dropped and one ends up with $\phi = (h/H)\sin\varphi$. This gives

$$1-\frac{m}{s} = \frac{1}{2}\langle\phi^2\rangle = \frac{h^2}{2H^2}\langle\sin^2\varphi\rangle = \frac{h^2}{4H^2}. \tag{3.37}$$

Eqs. (3.36) and (3.37) are confirmed by numerical results with high accuracy, see below.

3.1.5 Zero-field susceptibility

To have some reference point for comparison with numerical results, it is important to have the zero-field susceptibility of the Imry-Ma state. Application of a small field $H \to 0$ in the x direction slightly perturbs $\phi(\mathbf{r})$ created by the random field,

$$\phi(\mathbf{r}) \to \phi(\mathbf{r}) + \delta\phi(\mathbf{r}). \tag{3.38}$$

Linearization of Eq. (3.30) gives

$$Jsa^2\nabla^2\delta\phi - H\sin\phi = h\delta\phi\cos(\phi-\varphi). \tag{3.39}$$

Neglecting the rapidly oscillating small term in the right-hand-side of this equation we obtain in $3d$

$$\delta\phi(\mathbf{r}) = -\frac{H}{Jsa^2}\int d^3r' \frac{\sin(\mathbf{r}')}{4\pi|\mathbf{r}-\mathbf{r}'|}. \tag{3.40}$$

The magnetization per spin in the direction of the field is given by

$$\begin{aligned}\frac{\langle m\rangle}{s} &= \langle\cos\phi\rangle = -\langle\delta\phi\sin\phi\rangle \\ &= \frac{H}{Jsa^2}\int d^3r' \frac{\langle\sin\phi(\mathbf{r})\sin\phi(\mathbf{r}')\rangle}{4\pi|\mathbf{r}-\mathbf{r}'|}.\end{aligned} \tag{3.41}$$

This can be related to

$$\begin{aligned}\langle\mathbf{s}(\mathbf{r})\cdot\mathbf{s}(\mathbf{r}')\rangle &= s^2\langle\cos\phi(\mathbf{r})\cos\phi(\mathbf{r}')+\sin\phi(\mathbf{r})\sin\phi(\mathbf{r}')\rangle \\ &= 2s^2\langle\sin\phi(\mathbf{r})\sin\phi(\mathbf{r}')\rangle.\end{aligned} \tag{3.42}$$

Consequently,

$$\begin{aligned}\frac{m}{s} &= \frac{H}{2Js^3a^2}\int d^3r' \frac{\langle\mathbf{s}(\mathbf{r})\cdot\mathbf{s}(\mathbf{r}')\rangle}{4\pi|\mathbf{r}-\mathbf{r}'|} \\ &= \frac{H}{2Jsa^2}\int d^3r' \frac{\exp(|\mathbf{r}-\mathbf{r}'|/R_f)}{4\pi|\mathbf{r}-\mathbf{r}'|}.\end{aligned} \tag{3.43}$$

Integration gives

$$\frac{m}{s} = \frac{H}{2Js}\left(\frac{R_f}{a}\right)^2. \tag{3.44}$$

Zero-field susceptibility defined through

$$\frac{m}{s} = \chi \frac{H}{Js} \tag{3.45}$$

is given by

$$\chi = \frac{1}{2}\left(\frac{R_f}{a}\right)^2 = 128\pi^2 \left(\frac{Js}{h}\right)^4. \tag{3.46}$$

In the limit of small h this is very large, which may have prompted some statements in the past about infinite susceptibility of the Imry-Ma state. [50] As we shall see below, the actual zero-field susceptibility in a zero magnetization state is dominated by the dynamics of vortices and is much smaller.

Note that the initial magnetization of the Imry-Ma state in the limit of a very weak field and the approach to saturation at a higher field can be presented as

$$\frac{m}{s} = \frac{1}{2}\left(\frac{R_f}{R_H}\right)^2, \quad R_H \gg R_f \tag{3.47}$$

$$1 - \frac{m}{s} = \frac{1}{2}\left(\frac{R_H}{R_f}\right), \quad R_H \ll R_f, \tag{3.48}$$

where R_H and R_f are given by equations (3.32) and (3.20) respectively. Both formulas provide $m \sim s$ at $R_H \sim R_f$, which translates into

$$\frac{H}{Js} \sim \frac{1}{256\pi^2}\left(\frac{h}{Js}\right)^4. \tag{3.49}$$

For a weak random field, $h < Js$, this gives a very small value of H. It has the following physical meaning. If one studies the full hysteresis loop of the random-field system then the state close to saturation must have no vortices. In this case Eq. (3.48) is exact. Thus, the field in Eq. (3.49) provides the estimate of the maximal width of the hysteresis loop. In the limit of small h the loop must be very narrow, which is confirmed by our numerical

results. For small h one should use a very small field step in order not to confuse a very steep magnetization curve with a discontinuity in the magnetization curve. When the width of the hysteresis loop is so small that it cannot be resolved in either real or numerical experiment, its slope may well be described by Eq. (3.46).

3.1.6 Average magnetization of a finite system

As described in Section 1.2, we must be careful to distinguish between states with ferromagnetic order and those with a small magnetization due to statistical fluctuations in a finite system. Eq. (1.17) gives an equation for the magnetization of a finite system in terms of the correlation function, $C(\mathbf{R})$.

Substituting $C(\mathbf{R}) = s^2 \exp(-R/R_f)$ (no long-range order) into Eq. (1.17) in $3d$, one obtains

$$m = s \left(\frac{8\pi R_f^3}{V} \right)^{1/2} = \sqrt{8\pi}\, s \left(\frac{R_f}{L} \right)^{3/2}, \tag{3.50}$$

where L is the size of the system, $N = (L/a)^3$. At, e.g., $h = 0.5Js$, the Imry-Ma correlation length is $R_f \approx 200a$. For $L = 1000a$ this gives $m \approx 0.45s$. Such a large value of m for a not very weak random field in a system of the maximum size that we can access numerically suggests that any evidence of the long-range ferromagnetic order based upon finite m should be dealt with with care. However, LRO, if it is present, reduces the value of the $1/V$ term in Eq. (1.17).

3.1.7 Correlated random field

All the above formulas have been written for the uncorrelated random field described by Eq. (2.2) and $\Gamma(r) = \delta(r)$. Meanwhile, in physical problems involving flux lattices and random magnets, the static randomness can be correlated over a certain distance $\rho > a$. It is easy

to see that this leads to the following modification of R_f in Eq. (3.17):

$$\frac{R_f}{a} = \frac{16\pi a^3}{\Omega}\left(\frac{Js}{h}\right)^2, \tag{3.51}$$

where

$$\Omega = \int d^3 r \Gamma(r) \tag{3.52}$$

is the correlated volume, with $\Gamma(r)$ describing the short-range correlations of the random field.

For uncorrelated random field one has $\Omega = a^3$ and Eq. (3.51) goes back to Eq. (3.20). In the case of a correlated random field $\Omega > a^3$ and R_f is reduced. For, e.g., $\Gamma = \exp(-r/\rho)$, one obtains $\Omega = 8\pi\rho^3$ and

$$\frac{R_f}{a} = 2\left(\frac{a}{\rho}\right)^3\left(\frac{Js}{h}\right)^2. \tag{3.53}$$

Notice that the reduction in R_f is by a factor $8\pi(\rho/a)^3$ which can be quite significant. This, in principle, may allow one to test the effect of a very small h in a finite-size system. When the above formulas produce $R_f < \rho$, this means that $R_f = \rho$.

While we do not do a detailed numerical analysis with correlated random fields, a similar argument can be made for random anisotropy, which we analyze in detail with correlated randomness in Chapter 5.

3.2 Numerical results

3.2.1 General results

Our main finding is that for a weak random field the state of the system is always a glassy state with many local energy minima, so that the final state that we find depends on the initial state or initial condition, as well as somewhat on the details of the relaxation protocol.

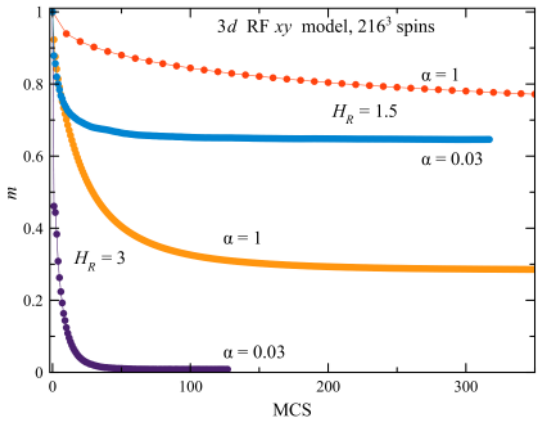

Figure 3.1: Magnetization relaxation curves starting from a collinear initial condition. The method with a small damping constant, $\alpha = 0.01 - 0.03$ is most efficient.

This to a some degree disqualifies earlier attempts to describe the random-field system by a unique magnetic state. Instead, the system exhibits magnetic hysteresis similar to that in conventional ferromagnets with pinning of the domain walls.

Starting from random initial condition we find states having small values of m (decreasing to zero in the large-size limit) and substantial vorticity. For $R_f \gg 1$ there is a strong short-range order everywhere except the vicinity of vortex loops. The correlation function in this state decays to zero but the correlation length is defined by the average distance between the vortices rather then by R_f, the former being much shorter. We call this state a vortex glass (VG).

Starting from collinear initial condition, for $H_R \lesssim 2$ we find only partially disordered states with m remaining of order 1 (stable in the large-size limit) and zero or extremely small vorticity. In this state, the correlation function follows Eq. (3.20) at short distances but reaches a plateau at longer distances, thus showing a long-range order. As the system does not order spontaneously upon cooling, but instead freezes into the vortex glass state described above, this behavior is analogous to a traditional permanent magnet with defects. We call this state ferromagnetic, but like a permanent magnet, accessing the magnetized

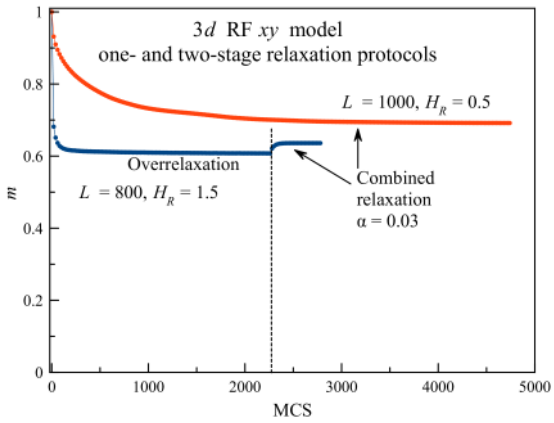

Figure 3.2: Two-stage relaxation starting from a collinear state for $H_R = 1.5$ and $L = 800$ and one-stage relaxation for $H_R = 0.5$ and $L = 1000$, our largest system size. Note a slow relaxation for $H_R = 0.5$.

state requires field cooling.

For $H_R \gtrsim 2$, starting from the collinear initial state, vortex loops are spontaneously generated and magnetization is strongly reduced.

The energy of the VG state is always higher than the energy of the ferromagnetic state. (This holds for both xy and Heisenberg models in $1d$, $2d$, and $3d$, as well as for random-anisotropy models.) Thus the vortex glass state is a metastable state that could, in principle, relax to the ferromagnetic state by eliminating vortex loops that cost energy. However, this does not happen because vortex loops are pinned by the random field. It is possible that the ferromagnetic state is also a metastable state, while there is a true ground state with $m = 0$, in accordance with the implicit theorem by Aizenman and Wehr[3, 43]. It should be noted that other work[51] has found a lower energy state with $m = 0$ for the Heisenberg model in three dimensions. However, accessing this state requires sweeping the external field many times, slowly lowering the width of the sweep to zero, so it is not accessible by simple means. We have been unable to find such a state using this method or any other. In fact, sampling local energy minima shows that, starting with a low m state, it is easier to find lower energy states with higher m than with lower m.

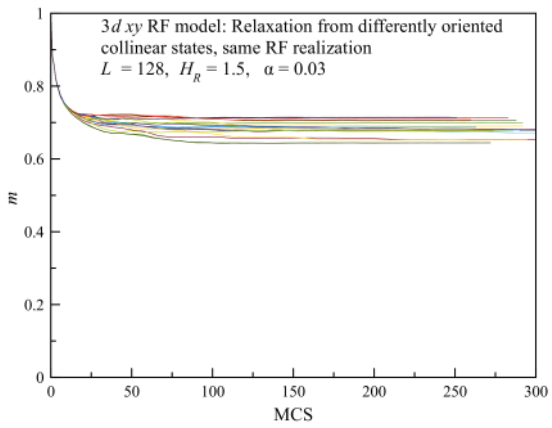

Figure 3.3: Relaxation starting from differently oriented collinear states for the same realization of the random field, showing glassy nature of the RF magnet.

3.2.2 Relaxation from the collinear state leading to the "ferromagnetic state"

During relaxation from any of the initial states we have tried, the system's energy decreases. Starting from collinear initial condition, m decreases until it reaches a constant value for $H_R \lesssim 2$ and goes to zero at $H_R \gtrsim 2$. Direction of the magnetization vector $\mathbf{m}$ practically does not deviate from the initial direction. Fig. 3.1 shows relaxation curves for $H_R = 1.5$ with m approaching a nonzero constant and for $H_R = 3$ with m going to zero. One MCS (Monte Carlo Step) means one complete spin update of the system. We use this standard notation although we are not using Monte Carlo. One can see that the pure finite rotation method ($\alpha = 1$) is slow for our problem in comparison to the combined method predominantly using over-relaxation ($\alpha = 0.03$). For $H_R = 3$, the system gets stuck in a metastable state with $m \approx 0.3$ and $\Delta E = -0.668$. However, the combined method finds the state with a very small m and the lower energy $\Delta E = -0.671$. Here $\Delta E \equiv E - E_0$, where $E_0$is the exchange energy of the collinear state, $-3J$ for the $3d$ model with periodic boundary conditions (pbc). These results are in accordance with the mechanism of relaxation sketched in Fig. 1.1.

In fact, already the pure over-relaxation method ($\alpha = 0$) provides a fast relaxation of m

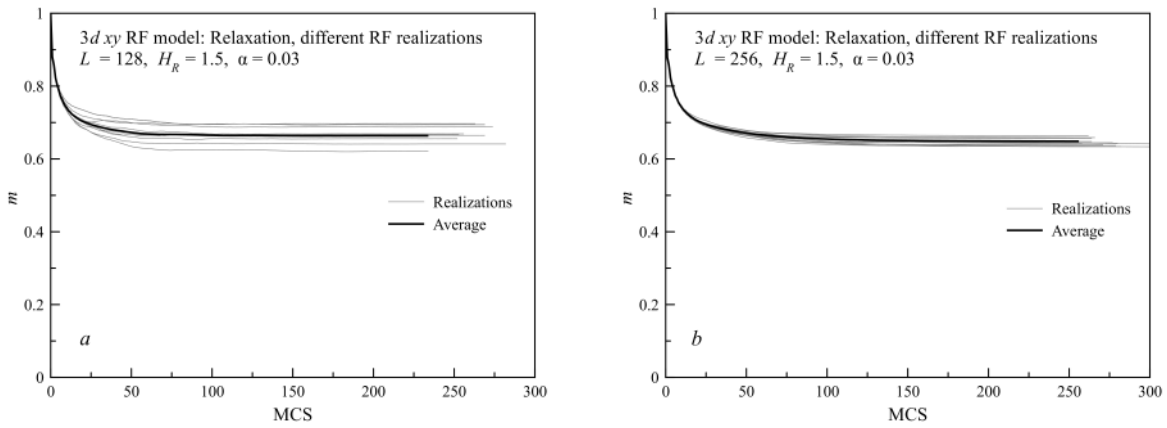

Figure 3.4: Relaxation from collinear states for different realization of the random field. Statistical scatter decreases with the system size due to self-averaging. a) $L = 128$; b) $L = 256$.

at a constant energy. For this reason in some computations we used the two-stage method, as shown in Fig. 3.2. The idea is that the conservative over-relaxation method has a potential for the maximal possible disordering since it leads to states that can be interpreted as thermal states with a small T (the over-relaxation plateau in Fig. 3.2). As the energy-relaxation mechanism is switched on, this temperature goes to zero and ordering in the system increases, as is seen in the Fig. 3.2. The states obtained in these computations are vortex free.

Fig. 3.3 obtained by multiple relaxation events of a system with *the same* realization of the RF from differently oriented collinear states shows different local energy minima achieved in different cases. This confirms glassy nature of a random-field magnet. All these states are vortex-free, as above.

Fig. 3.4 shows similar computations with different realization of the RF. One can see that Fig. 3.4*a* is similar to Fig. 3.3. Comparison of the two panels of Fig. 3.4 shows that the statistical scatter decreases with the system size because of self-averaging. For the standard deviation Δm of the magnetization in the final state one has $\Delta m \approx 0.025$ for $L = 128$ and $\Delta m \approx 0.0097$ for $L = 256$. On the other hand, $\Delta m L^{3/2} \approx 36$ for $L = 128$ and $\Delta m L^{3/2} \approx 39$ for $L = 256$ that are nearly the same. This is in accord with the picture of correlated regions

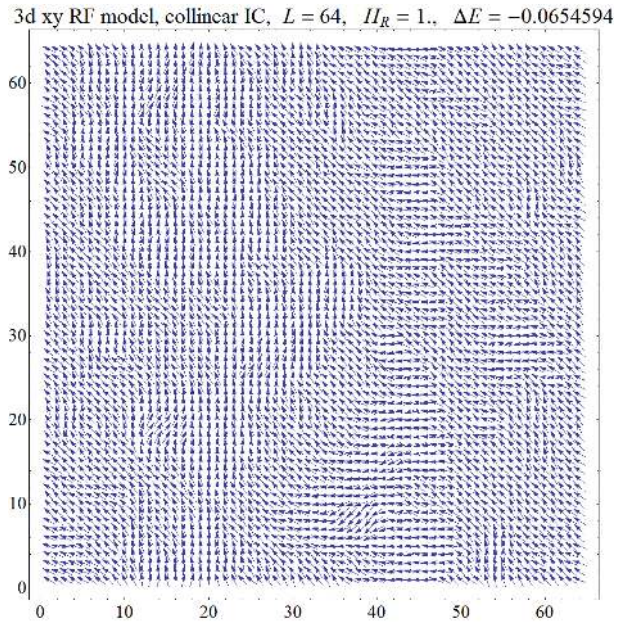

Figure 3.5: Spin configuration obtained for $H_R = 1$ from the collinear initial condition

of linear size R_f that are oriented independently from each other, leading to

$$\Delta m \propto \left(\frac{R_f}{L}\right)^{3/2}. \tag{3.54}$$

Using R_f of Eq. (3.17) and the numerical factor from the computational results above, one can estimate the statistical scatter in all other cases.

The structure of the ferromagnetic state shown in Fig. 3.5 has no singularities.

With increasing the system size the numerically found m does not decrease to zero, as one can see by comparing Figs. 3.1 and 3.2. The stability of the ferromagnetic state is clearly seen from the finite-size analysis shown in Fig. 3.6. Here all points except for $L = 800$ have been obtained by averaging over realizations of the random field, the number of realizations indicated by the italicized numbers. Although there is self-averaging in the system, averaging over realizations allows to further reduce data scatter. One can see that the points fall on straight lines with a finite offset, in accordance with Eq. (1.17). The error bars are the uncertainties of the average values computed as $\Delta m/\sqrt{n}$, where Δm is the

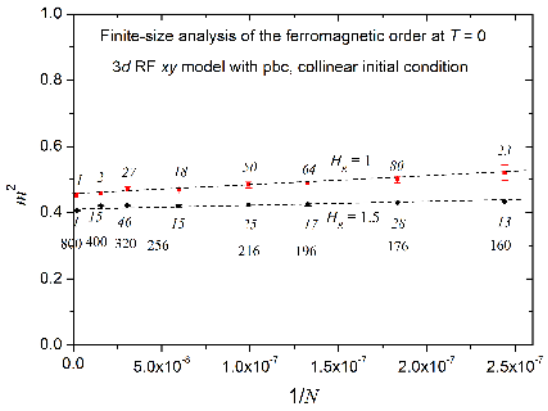

Figure 3.6: Magnetization squared in the ferromagnetic state vs system volume $V = N$. Italicized numbers are those of RF realizations used to compute the averages of m. Upright numbers below points indicate the systems' linear size L. Straight dashed lines are guides for the eye.

standard deviation defined by Eq. (3.54) and n is the number of realizations.

3.2.3 Relaxation from the wavy state

One can argue that the ferromagnetic state obtained from the collinear initial state is an artefact and ferromagnetism here is preselected. An argument in support of ferromagnetic state can be obtained by starting from a special kind of initial state that has $m = 0$ and no vortices or helicity. In this state, which we call a wavy state, spins rotate in one direction and then in the opposite direction when the observer is moving in any of the three directions in the cubic lattice. It is defined by

$$(s_x, s_y) = (\cos(\Phi), \sin(\Phi)), \tag{3.55}$$

where

$$\Phi = \frac{2\pi k_x n_x}{N_x} (-1)^{[k_x n_x / N_x]} + (x \Rightarrow y) + (x \Rightarrow z). \tag{3.56}$$

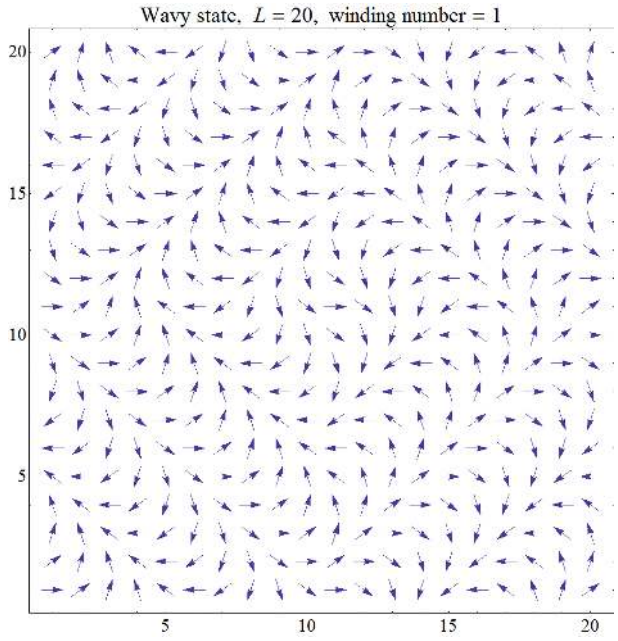

Figure 3.7: Wavy state of spins in the xy plane

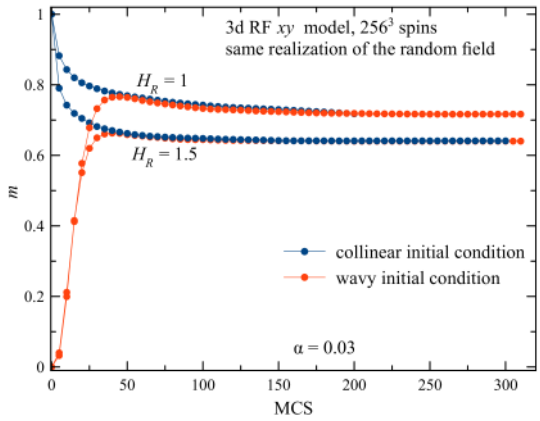

Figure 3.8: Magnetization relaxation from the collinear and wavy initial states.

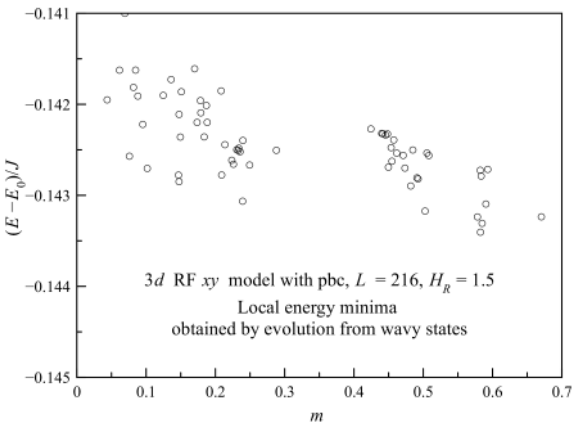

Figure 3.9: Local energy minima, labelled by the corresponding magnetization values, obtained by evolution from wavy states, Eq. (3.55), with $k_{x,y,z} = 0, 1, 2, 3$.

Here $N_{x,y,z}$ are lattice sizes, $n_{x,y,z} = 1, \ldots, N_{x,y,z}$ are lattice positions, $k_{x,y,z}$ are corresponding wave vectors and $[x]$ means integer part. The wavy state is topologically equivalent to the collinear state because it can be transformed into the latter by continuous deformations without changing the topology. This state resembles a spring that tends to straighten when released. Its energy is $\sim J(a/L)^2$ above that of the collinear state. An example of a wavy state is shown in Fig. 3.7. Fig. 3.8 shows magnetization relaxation curves starting from the collinear and wavy initial conditions that lead to the same final state with a high m. It must be noted that restoration of a large m out of the wavy state does not always take place. For $H_R \gtrsim 2$ vortices are generated spontaneously out of any vortex-free state, including the wavy state, so that the final state is a vortex glass with m close to zero. Even for $H_R = 1.5$ the system randomly lands in (vortex-free) states with small and large m, see Fig. 3.9. Note that states with higher m in Fig. 3.9 typically have a lower energy.

3.2.4 Vortex-glass state

The vortex-glass state contain singularities, vortices and antivortices, shown in Fig. 3.10. In our 3d case these are vortex lines going through the sample and vortex loops.

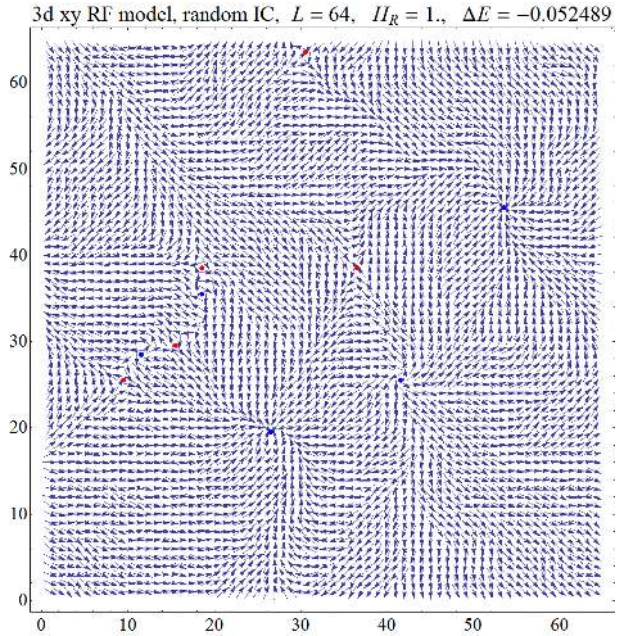

Figure 3.10: Spin configuration obtained for $H_R = 1$ from a random initial conditions. Vortices/antivortices are shown by blue/red circles.

For larger H_R vortex loops are created by the random field even starting from the collinear initial condition. For any system size, there is a critical value $H_{R,c} \approx 2$ above which vortex loops emerge. Slightly above $H_{R,c}$ these vortex loops are short, as shown in Fig. 3.11 (top). With increasing H_R, vortices quickly proliferate into the system and the number and length of vortex loops increase. It is difficult to prove whether there exists a size-independent threshold value $H_{R,c}$. Computations show that $H_{R,c}$ slowly decreases with the size. However, this question seems to be not very important because the vorticity increases with a very small slope above the threshold. It may be that in the bulk there are vortex loops at any finite H_R but the vorticity for small H_R is extremely low.

Meanwhile, starting from random initial conditions one arrives at states with long vortex lines that typically do not close into loops but cross the system's boundaries, see Fig. 3.11(bottom). As vortices and antivortices can exist in all three available planes, different singularities may exist at nearly the same point, e.g., a vortex in the xy plane may occupy

the same point as an antivortex in the yz plane. For this reason, some points in the figure may contain both black and red paints.

Obtaining VG states with our algorithm amounts to slow cooling the system. We have checked with Monte Carlo simulations that slow lowering the temperature leads to the same effect: the system does not order ferromagnetically but rather freezes into the VG state that for $H_R < H_{R,c}$ has a higher energy than the ferromagnetic state.

3.2.5 Magnetization and vorticity

The magnetization m and vorticity f_V as functions of H_R are shown in Fig. 3.12. Here the same realization of the random field was used and only its strength H_R was changed in small steps, using final states for a given H_R as initial conditions for the next value of H_R. Different random-field realizations result in slightly different curves.

At $H_R = 5$ vorticity is very high and it decreases upon lowering H_R. The magnetization remains very small as the system enters the vortex glass phase with a small but nonzero f_V. For $L = 216$ the number of vortex lines in the system becomes small below $H_R = 1$ [see Fig. 3.11(bottom)] and m starts to increase. For larger L, this happens at smaller H_R. In some cases the system reaches a collinear state with $m = 1$ at $H_R = 0$. In other cases, as in Fig. 3.12, the system ends up in a topologically stable state with nonzero helicity (for pbc) and $m < 1$.

The magnetization in the ferromagnetic state decreases with H_R as shown in Fig. 3.12, starting from the pure limit $m = 1$ at $H_R = 0$. For $H_R < 1.8$ this state is vortex-free. Proliferation of vortices for $H_R > 1.8$ results in the shoulder of this curve and full destruction of the order at $H_R > 4$.

The magnetization of the VG state for $H_R < H_{R,c}$ is small and it scales as $m \propto 1/L^{3/2}$, in accordance with Eq. (3.50), as shown in Fig. 3.13. Putting together data obtained for different L and H_R data, averaged over many RF realizations, one obtains the dependence

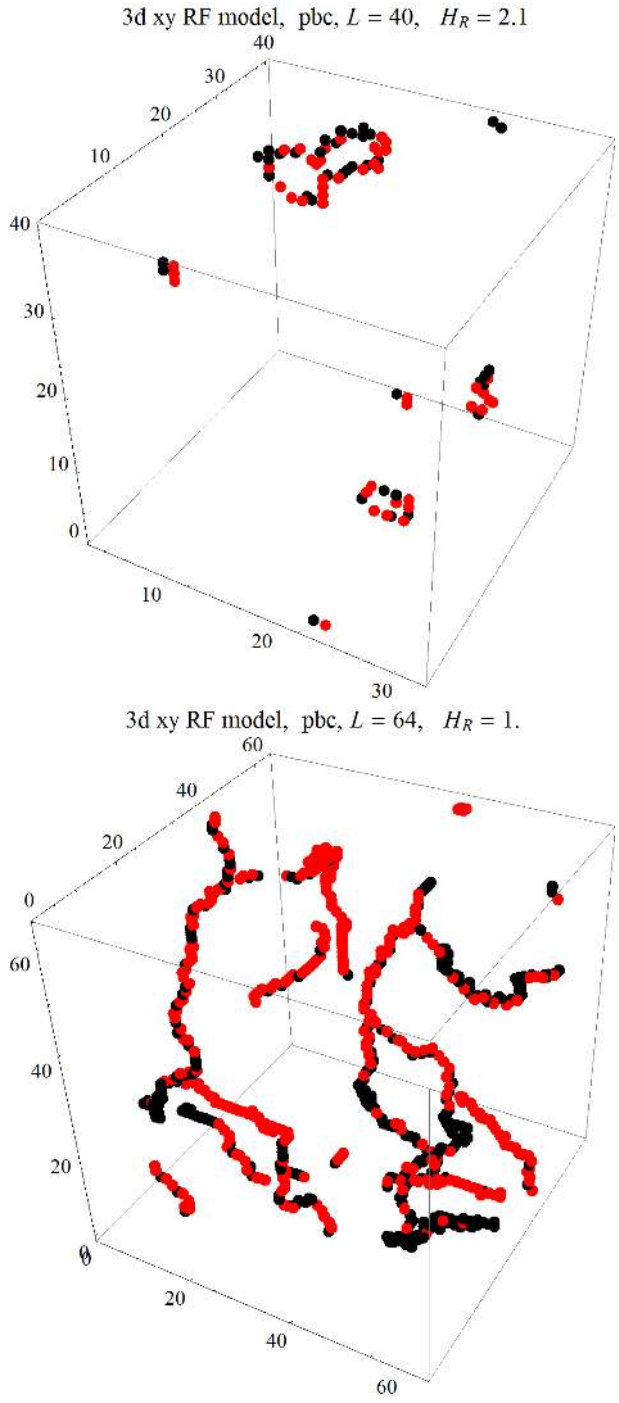

Figure 3.11: Vortex loops in 3d xy RF model. Collinear (top) and random (bottom) initial conditions. Vortices/antivortices are shown by black/red.

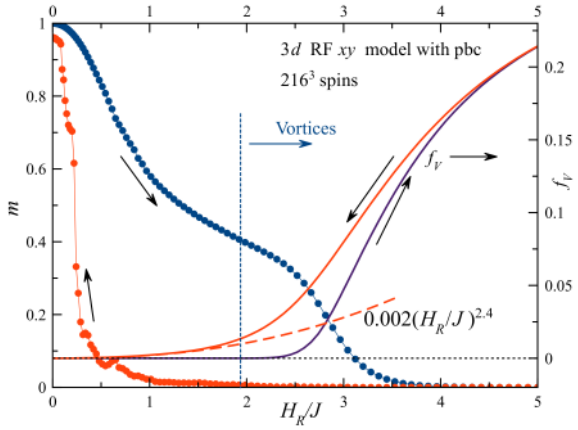

Figure 3.12: Magnetization vs the random field strength H_R for the model with pbc of the size $L = 216$.

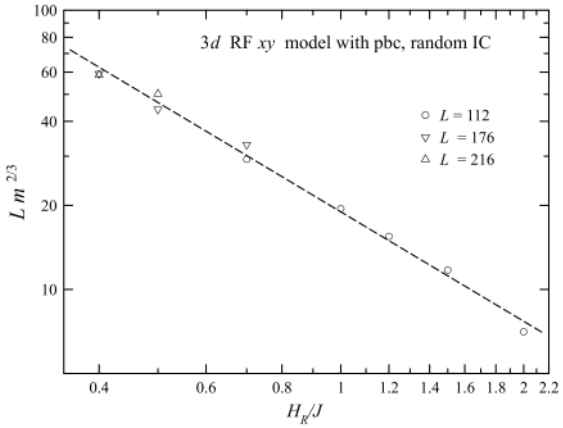

Figure 3.13: Finite-size analysis of the magnetization in the vortex-glass phase

of the correlation radius of the VG phase R_V that replaces R_f of Eq. (3.17). The result is

$$R_V \propto 1/H_R^{1.2} \tag{3.57}$$

that is much shorter than R_f at small H_R. The numerical factor in this formula cannot be found by this method because the form of the CF in the VG state is different from the simple exponential. The precise form of R_V will be found in the section on correlation functions below.

On the other hand, vorticity data in the VG state in Fig. 3.12 can be roughly fitted to the form

$$f_V \approx 0.002(H_R/J)^{2.4}. \tag{3.58}$$

Combining the two formulas above yields

$$R_V \propto 1/f_V^{1/2}. \tag{3.59}$$

It is clear that vortices are the main reason for the decay of spin-spin correlations in the vortex glass for $R_V \ll R_f$. Thus there must be a relation between R_V and the vorticity f_V defined as the fraction of unit plaquettes with vortices or antivortices. Naively one could expect that R_V is proportional to the distance between the singularities, so that in $3d$ one has $R_V \propto 1/f_V^{1/3}$. As vortex lines are linear objects, R_V is proportional to the average distance between vortex lines. This makes the situation effectively two dimensional.

3.2.6 Energy

Fig. 3.14 obtained from the same computation as Fig. 3.12 shows that the energy of the vortex-glass state is higher than the energy of the ferromagnetic state everywhere except

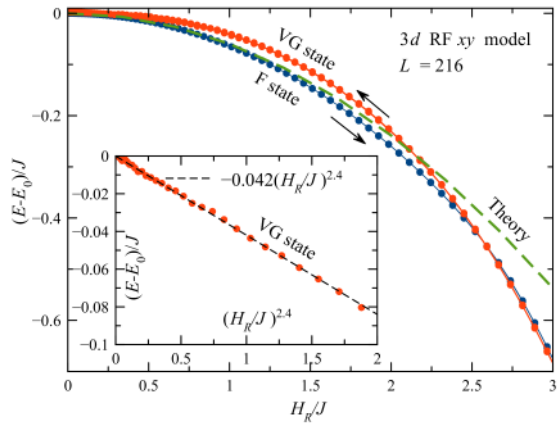

Figure 3.14: Energy vs the random field strength H_R in the ferromagnetic and vortex-glass states. The dashed green line labelled "theory" is Eq. (3.29). Inset: Fitting the energy in the vortex-glass state.

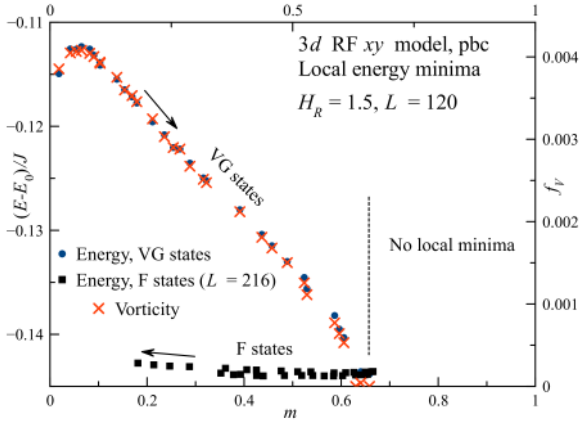

Figure 3.15: Energies of metastable vortex-glass states sampled vs their magnetization. Energy values in the vortex-glass state show a perfect correlation with their vorticities. Energies of vortex-free ferromagnetic states are comparable to those in Fig. 3.22.

for $H_R > 2.5$ where creation of vortices becomes energetically favorable. However, at these large values of H_R the destruction of the ferromagnetic state begins, see Fig. 3.12. Thus the vortex-glass state is metastable in the most interesting region of small H_R. The energy of the ferromagnetic state follows Eq. (3.29) in the range $H_R \lesssim J$. The energy per spin in the vortex-glass state can be fitted to

$$E - E_0 \approx -0.042J(H_R/J)^{2.4} \approx -21 f_V J, \tag{3.60}$$

where Eq. (3.58) was used. Note that by forming vortices the system is lowering its energy with respect to the energy of the collinear state. At the same time, creating vortices in the ferromagnetic state costs energy.

We have studied the correlation between the energies of metastable states and their magnetizations and vorticities. For this purpose, for $H_R = 1.5$ and $L = 120$, we first allowed the system to relax towards states with a preset value of m_z by applying a self-adjusting field H as a Lagrange multiplier. Doing so, we moved from $m_z = 0$ to $m_z = 1$ starting from the random state at $m_z = 0$ and using the state with the preceding value of m_z as the initial condition for finding the state with the next value of m_z. In another computation, we moved from $m_z = 1$ to $m_z = 0$ starting from the collinear state at $m_z = 1$. For each of these states with preset m_z, we set H to zero so that the system falls into the nearest local energy minimum, using the larger-than-usual relaxation constant $\alpha = 0.1$. The energies and vorticities of the found metastable states are plotted in Fig. 3.15 vs m. While increasing preset m_z, we obtain VG states the vorticity of which perfectly correlates with their energy. While decreasing preset m_z, we obtain vortex-free ferromagnetic states with lower energies. An interesting finding is that there are no local energy minima for $m \gtrsim 0.65$ in this plot, so that for all preset m_z above this value the system typically slides into the deepest energy minimum with $m \approx 0.65$.

These results seem to be in contradiction with the theorem of Aisenman and Wehr [3, 43] stating that the system must have $m = 0$ in the ground state. One possibility to reconcile our findings with that theorem is this. Starting from a vortex-free state, such as the states with $m \approx 0.65$, one can argue that there can be very rare configurations of the random field that would energetically favor the formation of vortices. The vorticity in these states is very small and locally they are very close to the vortex-free states. However, even a very small but finite vorticity could destroy spin correlations at large distances and render $m = 0$. Such states are not found if one starts with the collinear initial condition because they require surmounting energy barriers. On the contrary, starting from random initial conditions one ends up in the states with a much larger vorticity and higher energy.

This argument is quite plausible in $2d$, where vortices are point objects. However, it is less transparent in $3d$, where there are vortex loops and vortex lines traversing the entire system. Configurations of the random field that favor long vortex lines should be statistically very rare and there must be many more short vortex loops. However, the concentration of such vortex loops should be very small so that they would not disturb the magnetic order at large distances as the vortex lines do. Thus it is not clear whether a very diluted gas of vortex loops in an infinite sample destroys the long-range order. If it does it would be more along the lines of the Bragg glass theory.

3.2.7 Approach to saturation, hysteresis and memory

Fig. 3.16, which shows approach to saturation for large H, is in accord with Eq. (3.36).

For a strong random field, such as $H_R = 3$ in Fig. 3.17, hysteresis curves have a standard form. The irreversibility is related to the energy barriers at the atomic scale that changes the systems' vorticity. The relation between vorticity and hysteresis is clearly seen in the Fig. 3.17. In the course of the reversal the magnetization m decreases down to zero and then grows in magnitude again (not shown).

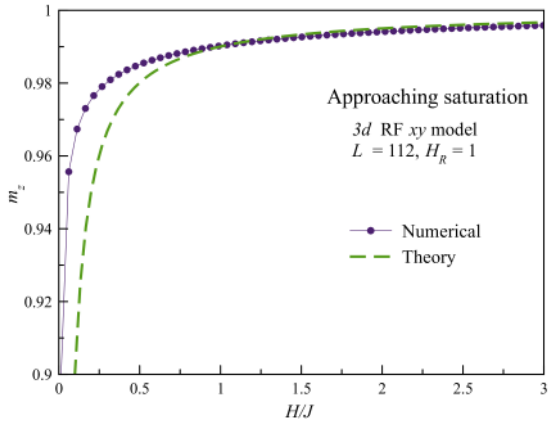

Figure 3.16: Approaching saturation in the $3d$ RF xy model. Dashed line is Eq. (3.36).

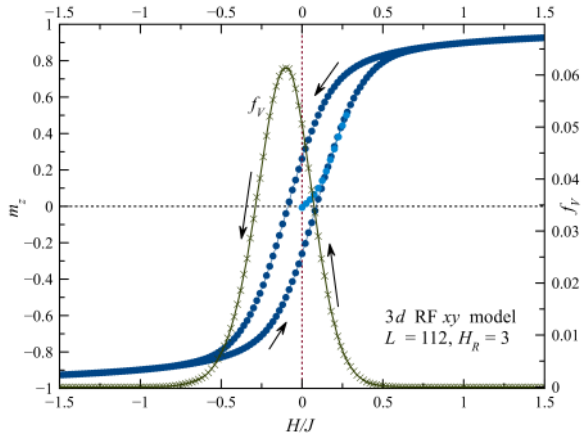

Figure 3.17: Hysteresis curves for $3d$ RF xy model for $H_R = 3$. Irreversibility is clearly related to vorticity.

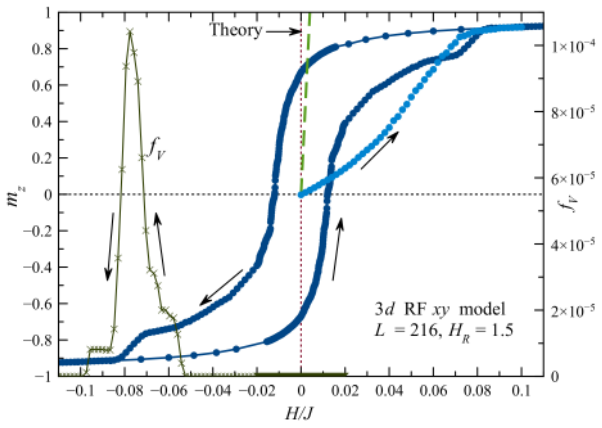

Figure 3.18: Hysteresis curves for $3d$ RF xy model for $H_R = 1.5$. The straight dashed line labeled "Theory" is based on Eq. (3.46). Dense and rarified points are results for different realizations of the random field. They overlap because of a sufficient self-averaging in the system.

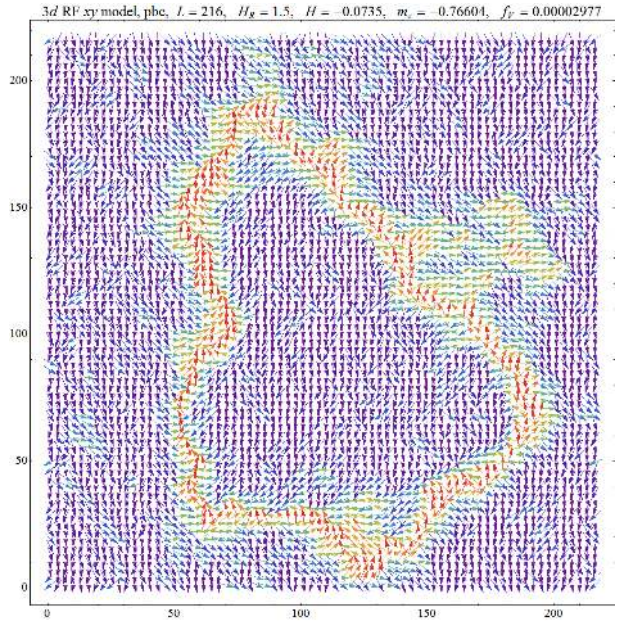

Figure 3.19: Walls of spins opposite to the field, pinned by the random field.

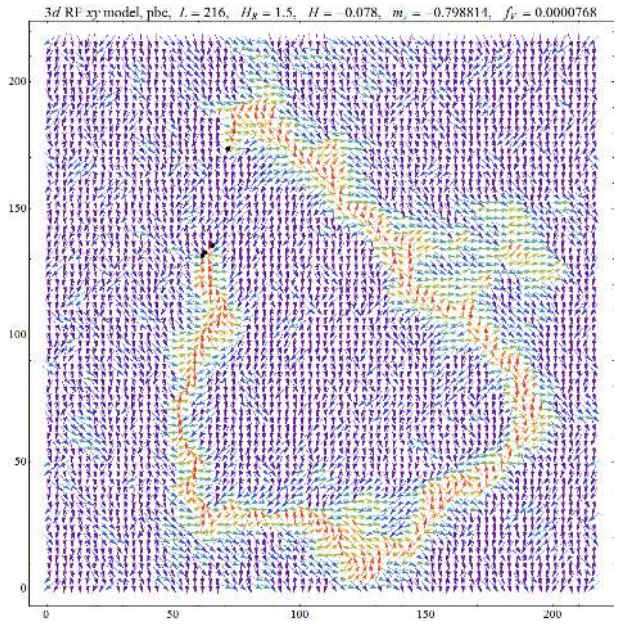

Figure 3.20: Walls of spins raptured by vortices (black points)

Fig. 3.18 shows hysteresis curves of a random-field xy magnet for $H_R = 1.5$ and $L = 216$. The initial magnetization curve that begins with $m_z = 0$ at $H = 0$ has a rather small slope, in a striking disagreement with large zero-field susceptibility that follows from the Green-function method, Eq. (3.46). This high rigidity of the vortex-glass state is due to the pinning of vortices that Imry-Ma scenario does not account for.

There is a large m at $H = 0$ along the H-down branch in Fig. 3.18 that does not depend strongly on the system size, which is in accord with Fig. 3.6. While the dependence of m_z on H along the hysteresis curve is rather steep at small fields, it is nearly smooth and has only small Barkhausen jumps (not seen in the figure), with the slope in the ball park of that given by Eq. (3.46). The magnetization of the sample does not rotate as a whole from positive to negative values of m_z. Instead, on average, the deviations of spins to the right and to the left from the positive z direction in different regions of space increase smoothly as H grows negative. In the process of spin reversal the regions with right and left spin deviations occupy rather large volumes separated by transient regions where spins are still

directed in the positive z direction. Such transient regions form walls of topological origin, see the cross-section of the sample in Fig. (3.19). They are pinned by the random field.

As the magnetization reversal proceeds along the hysteresis curve, the walls rapture, with the raptured area bounded by the vortex loop, as shown in Fig. 3.20. The loops then grow and eat the walls away, completing the reversal. This happens at $H = -H_V \approx 0.075$ in Fig. 3.18, where m_z has a shoulder and vorticity has a peak. Such a behavior is typical for the xy random magnet of size large compared to the ferromagnetic correlation length. Systems of smaller sizes typically switch their magnetization via rotation as a whole that leads to a jump from positive to negative values at a coercive field. This behavior is similar to that of a single-domain magnetic particle.

For $H > -H_V$, the upper hysteresis branch is quasi-reversible: Removing the field leads to partial restoration a large magnetization of the ferromagnetic state in $H = 0$, which can interpreted as a memory effect. The simulated relaxation curves are shown in Fig. 3.21. The recovery happens because the ferromagnetic state with spin walls exhibits elasticity. As the field is reversed, it stores energy and tends to return to the initial state when the stress due to the opposite field is removed. This behavior is a good evidence of the stability of the ferromagnetic state. The incomplete restoration of the magnetization in this experiment should be due to energy barriers not related to vortices.

The magnetization-recovery experiment provides an access to more ferromagnetic states than just relaxation from a collinear state. Because of small barriers there is a big number of metastable ferromagnetic states that differ by energy and magnetization m, shown in Fig. 3.22. States with smaller m occur due to relaxation from states with smaller m_z in the upper hysteresis branch in Fig. 3.18. This is also seen in Fig. 3.21. The rightmost state in Fig. 3.22 is obtained by relaxation from any state with $m \gtrsim 0.7$ because there are no local energy minima in this range. There is a significant interval of m values in the ferromagnetic states in Fig. 3.22, all having very close energies, in contrast with much larger energy differences

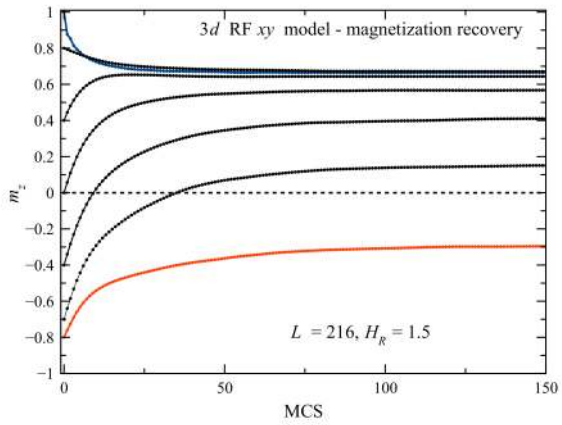

Figure 3.21: Magnetization recovery from the quasi-reversible branch of the hysteresis curve ($H > -H_V$ in Fig. 3.18), computed after setting $H = 0$. The red curve corresponding to the initial value $m_z = -0.8$ does not go into the positive region because this initial state is beyond the quasi-reversible branch and has a large vorticity.

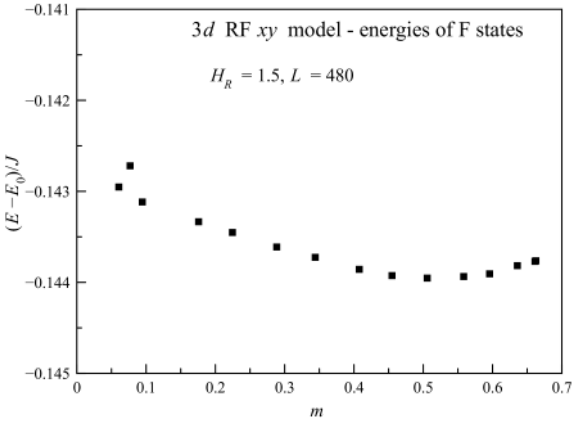

Figure 3.22: Energies of vortex-free ferromagnetic states (local energy minima) obtained by magnetization recovery of the type shown in Fig. 3.21. The rightmost state is obtained by relaxation from any state with $m \gtrsim 0.7$.

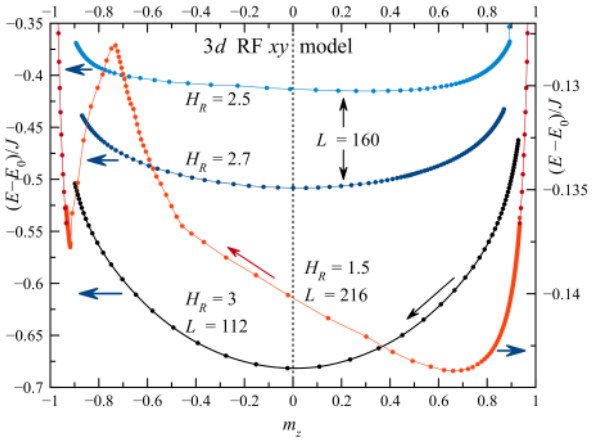

Figure 3.23: Energies of the states created by the external field H vs m_z (with the energy due to H subtracted). The lowest-energy state corresponds to $m_z = 0$ for $H_R \gtrsim 2.6$ and to $m_z > 0$ for $H_R \lesssim 2.6$.

between vortex-glass states in Fig. 3.15. One can clearly see that the lowest-energy state is at $m \approx 0.5$, a value that varies a bit depending on the random field realization. The energy values in Fig. 3.22 are comparable to those of the ferromagnetic states for $L = 216$ in Fig. 3.15 and the states in Fig. 3.9.

Another method of accessing the energies of the states vs their magnetization is to plot the energy obtained in the computation of the hysteresis (with the energy due to the external magnetic field H subtracted) vs m_z. In this way one can access not only local energy minima, as in Fig. 3.22 but also the energies of all unstable states supported by the external field. Fig. 3.23 shows the computed energies for different values of H_R. A striking feature is the transition between the energy minimum at $m = 0$ to an energy munimum at $m > 0$ on H_R that occurs at $H_R \approx 2.6$. One can see that for $H_R = 1.5$ the results are very close to those for the local energy minima in Fig. 3.22 but also contain unstable states with $m \gtrsim 0.7$. Suppression of ferromagnetic states at large H_R was already seen in Fig. 3.12. The energy maximum at $m_z \approx -0.8$ corresponds to the shoulder at this m_z in Fig. 3.18. On decreasing H_R, its increasing part is due to the energy input into compressed spin walls while its decreasing part and it is due to rapture of spin walls by vortex loops.

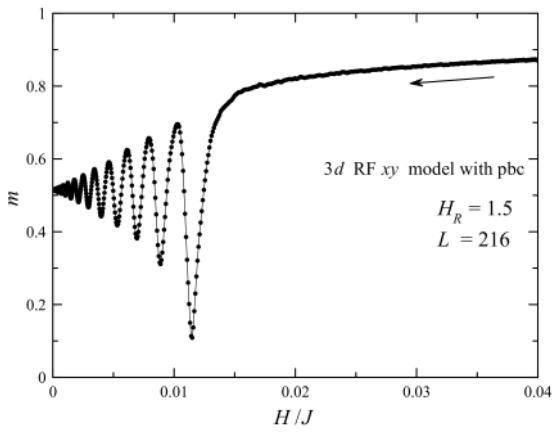

Figure 3.24: Magnetization vs decreasing magnitude of a rotating field **H**

3.2.8 Ordering by decreasing rotating field

Another type of numeric experiment showing ferromagnetic ordering is relaxation in the presence of a rotating external field **H** with the magnitude slowly decreasing to zero. This is a version of the method of *stimulated annealing* that helps the system to overcome barriers preventing it from relaxing to states with a lower energy. If there were states with a small or zero magnetization having a lower energy that in our other numerical experiments, these states were likely to be reached by this method.

Numerical results shown in Figs. 3.24 and 3.25 show that also in the decreasing rotating field experiment ferromagnetically ordered states are reached. For the field magnitude H large enough, the direction of **m** follows that of **H**, while both H and m are decreasing. As H goes below 0.015 (see Fig. 3.24), direction of **m** decouples from that of **H** and, after oscillations around an energy minimum corresponding to a significant value of m, the system reaches this energy minimum. In the above numerical experiment, the final magnetization value is $m = 0.5148$. It turns out that our method leads to the energy values very close to those of Fig. 3.22. Thus, no states with a smaller m and lower energy have been found, that again proves robustness of the ferromagnetically ordered state.

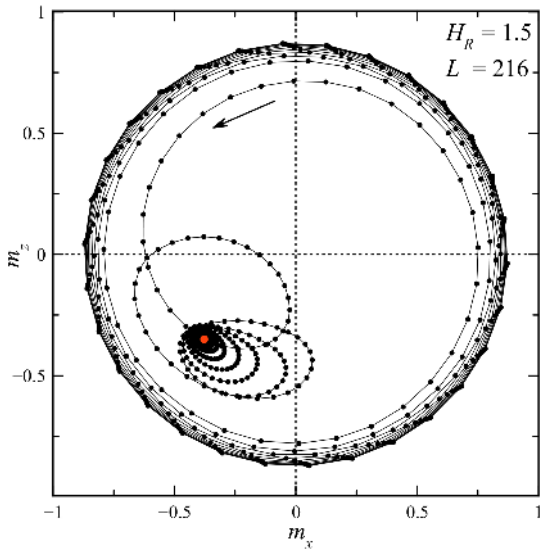

Figure 3.25: Components of the magnetization vector **m** in the rotating-field experiment

In another type of numerical experiment, a field slowly oscillating parallel to a fixed direction with the amplitude slowly decreasing to zero had been applied. Here one could obtain states with a small magnetization. However, the energy of such states was higher than the energy of the F state because of the vorticity generated by rapturing spin walls, see Sec. 3.2.7.

3.2.9 Correlation functions

We have computed correlation functions in the energy minima of our system that we have found by our relaxation algorithm. After computing CFs we averaged them over directions of $\mathbf{R} \equiv \mathbf{r}_1 - \mathbf{r}_2$.

In the vortex-glass state obtained from random initial conditions, correlation functions shown in Fig. 3.26 decay to zero but their form and correlation radius is different from Eqs. (3.20) and (3.17). The results can be fitted by the stretched exponential

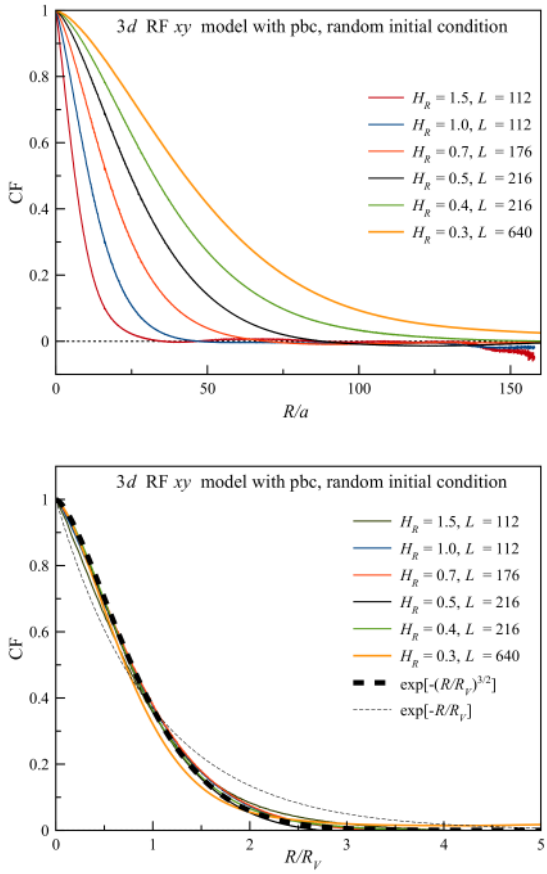

Figure 3.26: Correlation functions of the 3d RF xy model in the vortex glass state obtained starting from random initial conditions. Natural (top) and scaled (bottom) presentations. R_V is given by Eq. (3.61).

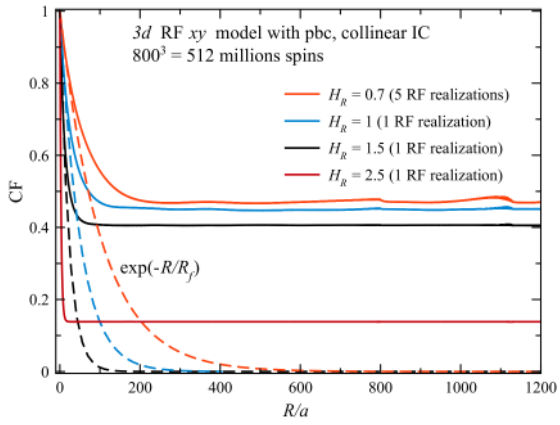

Figure 3.27: Correlation functions of the 3d RF xy model in the ferromagnetic state obtained starting from collinear initial conditions.

$$\langle \mathbf{s}(\mathbf{r}_1) \cdot \mathbf{s}(\mathbf{r}_2) \rangle = s^2 e^{-(|\mathbf{r}_1 - \mathbf{r}_2|/R_V)^{3/2}}, \quad R_V \simeq 14 \, (Js/H_R)^{1.2} \, . \tag{3.61}$$

Note that the dependence of R_V on H_R is much weaker than $R_f \propto 1/H_R^2$ of Eq. (3.17) and thus $R_V \ll R_f$ at small H_R. Using the vorticity dependence of Eq. (3.58), one can express the VG correlation length R_V as

$$R_V \simeq 0.6/f_V^{1/2}, \tag{3.62}$$

c.f. Eq. (3.59). This dependence is in agreement with the $2d$ nature of vortices discussed below Eq. (3.59).

If the initial state is collinear and H_R is not too large, the correlation functions have plateaus at large distances. At $R \lesssim R_f$ they exactly follow Eq. (3.20). The results for our largest size $L = 800$ are presented in Fig. 3.27. For $H_R = 1$ and 1.5 there is enough self-averaging and we show correlation functions obtained for only one random-field realization. They have well-defined plateaus with small fluctuations. For $H_R = 0.7$, correlation functions obtained with one random-field realization are too bumpy and averaging over realizations is needed. The bumps at $R = 800$ and $\sqrt{2} \times 800$ are artifacts of periodic boundary conditions. The length of the plateaus show that the large magnetization in the ferromagnetic state is not a fluctuational magnetization.

The perfect plateau for $H_R = 2.5$ shows that the appreciable vorticity $f_V = 0.01766$ in this state does not yet disrupt ferromagnetic order at long distances. This should be the consequence of vortices forming small closed loops such as in Fig. 3.11(top). Meanwhile, one can expect that even a small concentration of vortex lines that go through the whole sample, as is the case in the vortex-glass state, see Fig. 3.11(bottom), will destroy the long-range order.

3.3 The Imry-Ma argument and vortices

Surprising robustness of the ferromagnetic state found in our different calculation requires an explanation. According to the Imry-Ma scenario, starting from collinear state, spins would relax towards directions of the random field averaged over correlated regions of linear size R_f, so that the magnetization would go to zero if R_f is small compared to the size of the system. In our computations we indeed observe a fast initial disordering but then the magnetization stops to decrease at an appreciable value, Figs. 3.1 and 3.2. What could be the factor that prevents it from relaxing to zero?

The answer to this question seems to be that the magnetization cannot smoothly follow the average random field without the formation of vortices in $2d$ and vortex loops in $3d$. The latter cost energy that prevents relaxation towards a completely disordered state. Thus ferromagnetically ordered state is topologically protected.

This can be demonstrated by considering the average of the random field over the correlated region around each point $\mathbf{r}$, the so-called moving average, for instance,

$$\bar{\mathbf{h}}(\mathbf{r}) = \frac{1}{V_f} \int\limits_{|\mathbf{r}'| \le R_f} d^d\mathbf{r}' \mathbf{h}(\mathbf{r}' + \mathbf{r}), \tag{3.63}$$

where V_f is the correlated volume, $V_f = (4\pi/3)\, R_f^3$ in $3d$. This is exactly a mathematical implementation of the original Imry-Ma argument. The averaged random field $\bar{\mathbf{h}}(\mathbf{r})$ describes a disorder correlated at length R_f. Since its components $\bar{h}_x(\mathbf{r})$ and $\bar{h}_y(\mathbf{r})$ are sums of many random variables, they have a Gaussian distribution at any point $\mathbf{r}$ and are statistically independent. Spin field in the Imry-Ma state, aligned with $\bar{\mathbf{h}}(\mathbf{r})$, should be of the form

$$\mathbf{s}_{\mathrm{IM}}(\mathbf{r}) = \frac{\bar{\mathbf{h}}(\mathbf{r})}{\left|\bar{\mathbf{h}}(\mathbf{r})\right|}. \tag{3.64}$$

Now, it can be shown that such defined spin field has singularities. This happens when

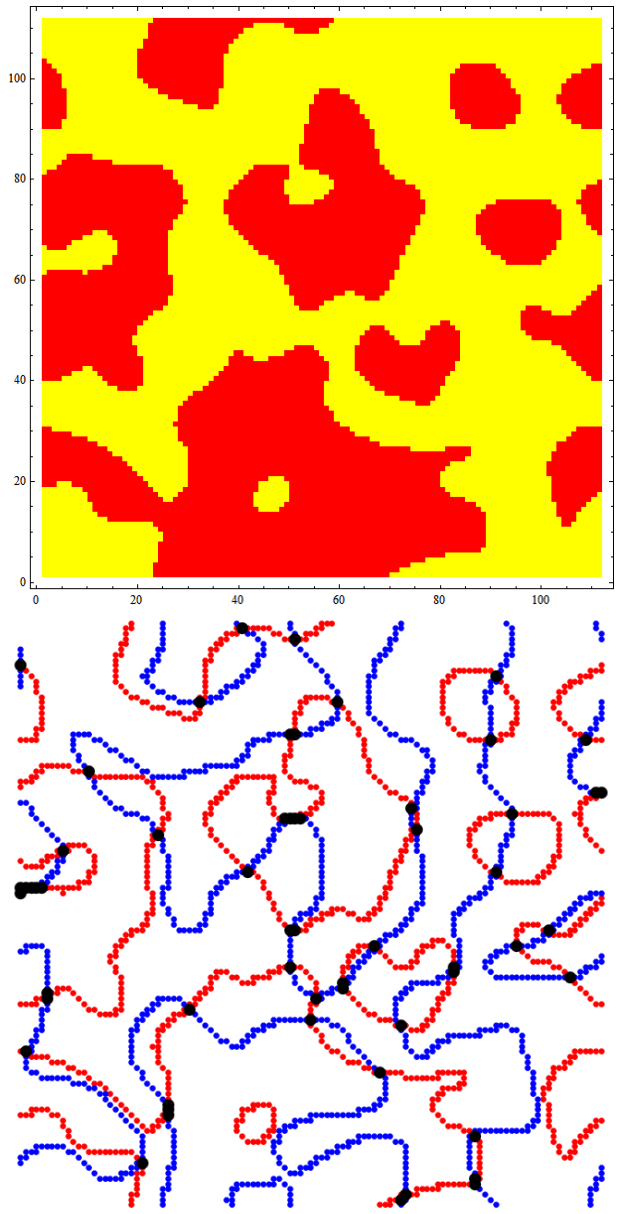

Figure 3.28: (Top) Domains of positive and negative $h_x(\mathbf{r})$ in a xy plane. (Bottom) Singularities at the crossings of domain boundaries for $h_x(\mathbf{r})$ and $h_y(\mathbf{r})$ in a xy plane.

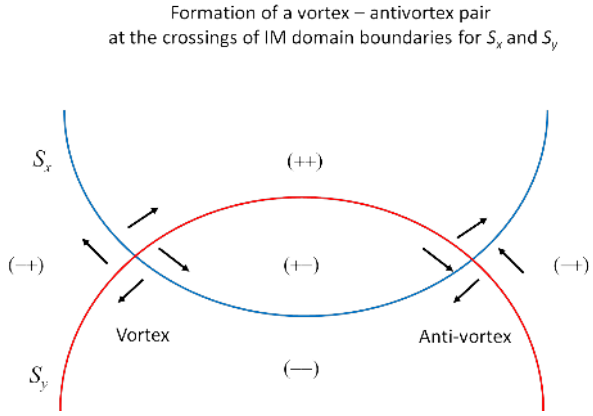

Figure 3.29: Formation of vortices and antivortices at the crossings of domain boundaries for $h_x(\mathbf{r})$ and $h_y(\mathbf{r})$.

$\left|\bar{\mathbf{h}}(\mathbf{r})\right| = 0$, that is, both components of $\bar{\mathbf{h}}(\mathbf{r})$ turn to zero. Regions of positive and negative $s_x(\mathbf{r})$ in a xy plane, generated by Eq. (3.64) are shown on Fig. 3.28. The areas of positive and negative $s_x(\mathbf{r})$ are on average the same and the boundaries between domains are random lines shown in Fig. 3.28(top). Domain boundaries for $s_y(\mathbf{r})$ are also random lines statistically independent from the former. Thus domain boundaries for $s_x(\mathbf{r})$ and $s_y(\mathbf{r})$ will cross at some points, as shown in Fig. 3.28(bottom). At these points vortices or antivortices will be generated because of the denominator in Eq. (3.64), as illustrated in Fig. 3.29. In $3d$ there will be vortex loops that cost much more energy than a vortex in $2d$.

Let us now estimate the energy gain in the IM state with vortices. There is about one vortex per IM domain with size R_f, having the energy

$$E_V \sim Js^2 \left(\frac{R_f}{a}\right) \ln\left(\frac{R_f}{a}\right). \tag{3.65}$$

The corresponding exchange energy per spin is

$$E_{\mathrm{ex}-V} \sim Js^2 \left(\frac{a}{R_f}\right)^2 \ln\left(\frac{R_f}{a}\right) \tag{3.66}$$

that should replace the first term in Eq. (1.8). Minimization with respect to R_f in the resulting energy expression gives

$$R_f \sim a \left(\frac{Js}{h}\right)^2 \ln^2\left(\frac{Js}{h}\right) \tag{3.67}$$

that is longer than the IM correlation radius because of the large lorarithm. The corresponding energy gain

$$E - E_0 \sim -Js^2 \left(\frac{h}{Js}\right)^4 \left[\ln\left(\frac{Js}{h}\right)\right]^{-3} \sim \frac{\Delta E_{IM}}{\ln^3(Js/h)} \tag{3.68}$$

is the IM energy gain divided by a large logarithmic term.

On the other hand, the ferromagnetic state we have found numerically can be understood as an incompletely disordered IM state, in which the energy gain is ΔE_{IM} reduced by a numerical factor of order one rather than by a large logarithmic term. The energy of this ferromagnetic state should be lower than that of the IM state with vortices, in accordance with our numerical results (see, e.g., Figs. 3.14 and 3.15). The rapid relaxation out of the collinear state followed by a plateau in Figs. 3.1 and 3.2 can be explained as follows. Spins are readily relaxing in the direction of the net RF in the regions of linear size R_f until their further rotation toward the totally disordered IM state requires creation of vortices. As the latter costs energy, relaxation stops at this point.

Of course, there is a non-zero probability that the random field at the location of the vortex is vortex-like and almost parallel to the spin field. In this case the energy gain from the vortex will be significantly higher. However, since the Imry-Ma state in which the spin field follows the direction of the average local random field is unique for every choice of the correlated volume V_f, so should be the positions of the vortices. The fraction of the lucky vortices mentioned above is determined by the probability of the corresponding lucky configuration of the random field, which is small. Consequently, it cannot affect the above argument .

3.4 Discussion

We have studied states of local energy minima of the random-field xy model focusing on weak random fields. The minimal random-field value $h \equiv H_R$ in our work is defined by $h/J = 0.3$, see Fig. 3.26. This should be considered weak for the following reason. In the cubic lattice each spin has six nearest neighbors that are nearly collinear for small h, the exchange field is $J_0 \equiv 6J$. Thus, physically it makes more sense to consider the dimensionless parameter h/J_0 that in our computations has the minimal value $h/J_0 = 0.05$ being manifestly small. In terms of J_0 formulas of the LIM theory do not contain large numbers. For instance, R_f in Eq. (3.17) can be rewritten as $R_f/a = (4\pi/9)(J_0 s/h)^2$.

Computations have been performed on lattices up to $1000 \times 1000 \times 1000$ spins. Our main finding is that completely disordered ($m \cong 0$) states are dominated by vortices and have higher energy than vortex-free ferromagnetically ordered states. There are unsurpassable energy barriers between different states even in the case of a weak random field because switching between different spin configurations involves large groups of correlated spins. This makes the magnetic states depend strongly on the initial conditions. At first glance this may appear conceptually similar to the behavior of a conventional ferromagnet with pinning of domain walls. Prepared with random orientations of spins, it would freeze in a state with small magnetic domains and high energy due to many domain walls. In a similar fashion, the random-field magnet freezes in a high-energy state due to many vortices pinned by the random field. When prepared with collinear spins, the conventional ferromagnet would remain in a magnetized state because pinning prevents domain walls from proliferating into the sample and achieving the ground state with zero total magnetization. Similarly, the random-field magnet prepared with collinear spins relaxes to a state with non-zero magnetic moment.

There is an essential difference between the two systems though. While the conventional

ferromagnet tends to relax toward an $m = 0$ state via diffusion of domain walls out of local energy minima, the random-field magnet in our computations does not have this tendency to relax to the zero-magnetization state out of the magnetized state. In fact the energies of zero-magnetization states found in our various types of computations are always higher than the energies of magnetized states. One possibility is that the zero-magnetization state is not the ground state. Another possibility is that there are energy barriers to relaxation out of the magnetized state that involve collective behavior of large volumes of spins and they are actually greater for a weaker random field. This would be very different from shallow local energy barriers for the diffusion of domain walls in conventional ferromagnets.

The bottom line of our analysis is that the Imry-Ma state in which the system breaks into finite-size domains providing zero total magnetic moment is impossible without formation of vortex loops. They become very long and possess very large energy when the random field becomes very small. This makes the barriers associated with the formation of the zero-magnetization state unsurpassable at any temperature even in the limit of weak random field. The above argument is based upon h-dependence of R_f and it stands as long as R_f is small compared to the size of the system. One can ask how close the vortex-glass state is to the Imry-Ma state. To address this question, for $H_R = 1.5$ we have created an Imry-Ma state of Eq. (3.64) and let it relax. As the result, the vorticity decreased from $f_V \approx 0.008$ in the Imry-Ma state to $f_V \approx 0.0006$ in the vortex-glass state. This means that the system tries to annihilate vortices to reduce its energy but it cannot do it completely because some vortices are pinned. Similar conclusion regarding dislocations in two-dimensional pinned flux lattices has been reached in Ref. [52].

On the other hand, it must be stressed that the ground state of the system was not systematically searched for, and, moreover, it is of little relevance in glassy systems. A single vortex loop going across the whole sample will totally destroy magnetic order while its excess energy, as well as its vorticity, will be vanishingly small. It cannot be excluded

that such type of states has the lowest possible energy. However, these states are exotic and they were not studied here. Consequently, we cannot rule out the existence a completely disordered vortex-free ground state in our computations. However, finding such a state may require a special initial condition or a more sophisticated numerical argorithm anticipating the result.

It is generally believed, see, e.g., Refs. [46, 48], that in the presence of quenched randomness the elastic interactions, like the ones in the atomic or vortex lattices, or exchange in spin lattices, provide the elastic-glass ground state that is characterized by the power law decay of correlations at large distances. We have not found such a behavior for the random-field xy spin model in three dimensions. The relation between that model and randomly pinned flux lattices in superconductors has been discussed in some detail in Ref. [47]. The role of topological defects in flux lattices is played by dislocations as compared to vortices in spin models. Large areas of defect-free flux lattices have been observed in experiment, see, e.g., Ref. [6]. When analyzing such experiments, one should remember, however, that for weak disorder the correlation length in $3d$ can be very large, making it difficult to distinguish large defect-free slightly disordered domains from the Bragg glass. While it is possible that some of the conclusions of this paper apply to pinned flux lattices the latter requires a separate study because the two models have different symmetry and different kinds of interaction with the random field.

Chapter 4

The effect of a dilute random field on a continuous-symmetry order parameter

In this chapter, we focus on a variation of the random field problem that is particularly relevant to real-world systems. Random fields themselves generally don't arise naturally in pure ferromagnetic systems[54], but there are many systems where dilute impurities may create fields, creating quenched randomness in the system. In this case, Eq. (2.1) is altered so that the random field $\mathbf{h}(\mathbf{r})$ is zero, except at $N \cdot c_r$ points in space where impurities are located. For the sake of numerical work in this chapter, we will assume $h \gg J$ and $h \gg H$, but we will see that, as long as the fraction of sites with impurities $c_r \ll 1$, the system will show non-trivial behavior.

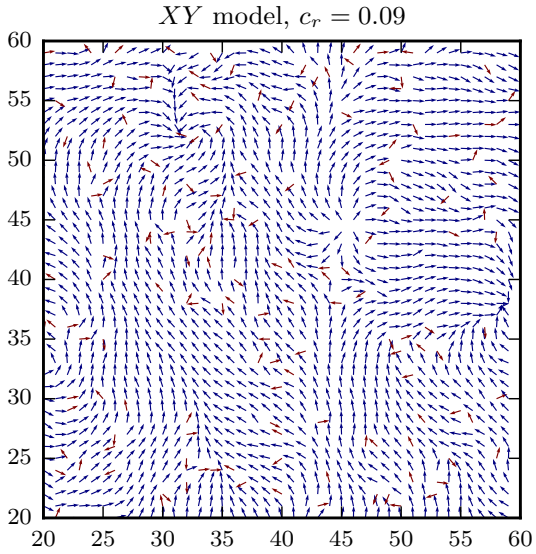

Figure 4.1: Snapshot of XY spins in one layer of a $3d$ lattice after relaxation from random initial orientation in the presence of dilute random field. Spins whose orientations are frozen by the random field are shown in red.

4.1 Numerical Results

We begin with the evolution of the system from random initial orientation of spins. The randomly chosen c_r fraction of spins remain frozen in random directions, while other spins are allowed to rotate and relax to some final state in which the total magnetization is no longer changing. A snapshot of such a state is shown in Fig. 4.1. The presence of topological defects and short-range order is apparent. The corresponding spin-spin correlation function and its fit by the exponential are shown in Fig. 4.2. This fit allows one to extract the ferromagnetic correlation length R_f. Its dependence on the concentration of impurities, c_r, is shown in Fig. 4.3. The $1/c_r$ dependence of R_f provides a good fit to the numerical data for both the XY model with two spin components and the Heisenberg model with three spin components.

The state obtained by the relaxation from collinear initial conditions (with all spins

This chapter is based on work originally presented in Ref. [53]

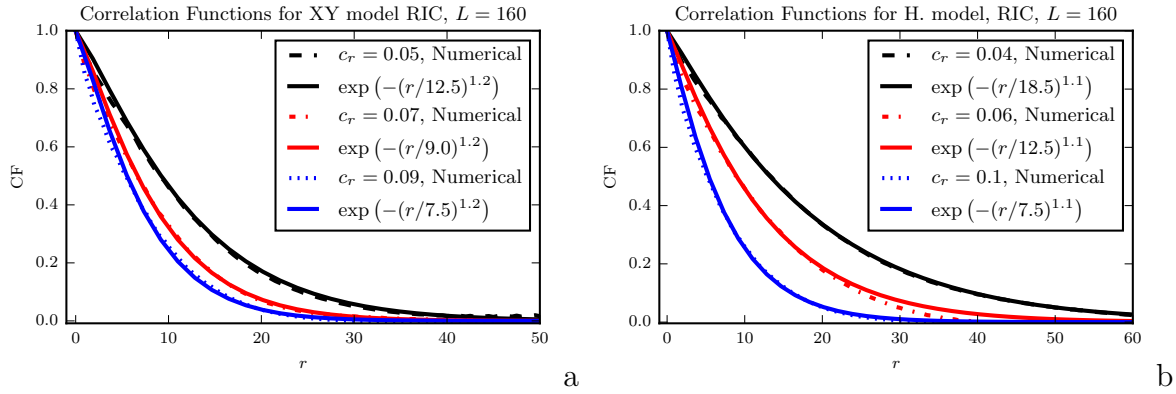

a b

Figure 4.2: Spin-spin correlation function (dashed lines) after relaxation from random initial orientation of spins in the presence of dilute random field. Solid lines provide the corresponding fit by the exponential. Distances are given in lattice units, with L being the size of the $L \times L \times L$ system. a) $3d$ XY spin model. b) $3d$ Heisenberg spin model.

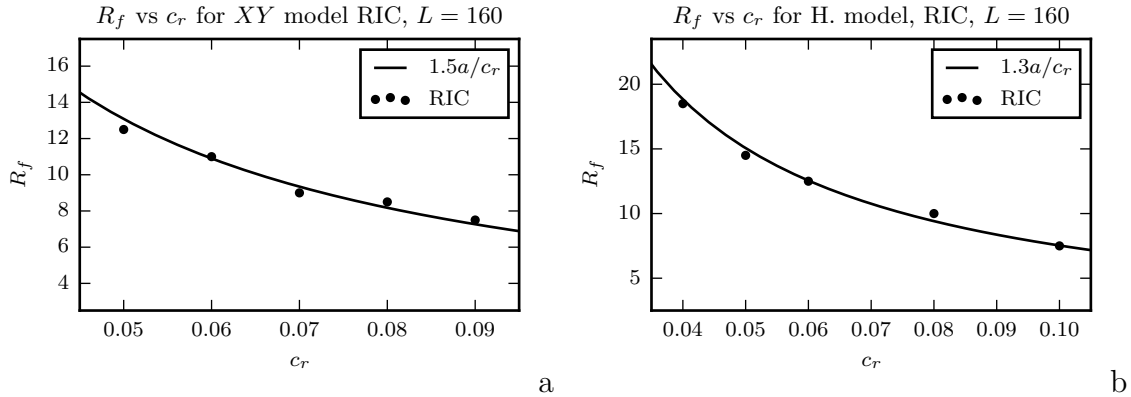

a b

Figure 4.3: Dependence of the ferromagnetic correlation length on the concentration of random field sites for the state obtained by evolution from random initial orientation of spins. a) $3d$ XY spin model. b) $3d$ Heisenberg spin model.

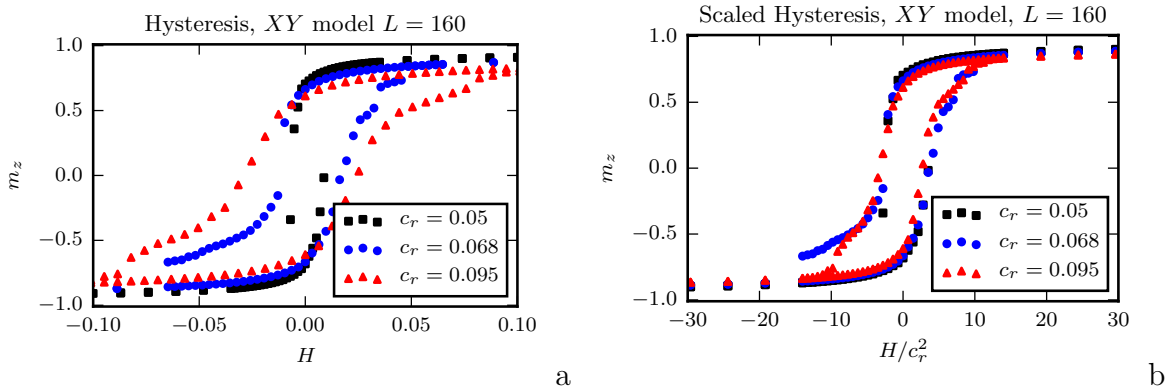

a b

Figure 4.4: Hysteresis loops for the $3d$ XY model with dilute strong random field for different concentrations of the random-field sites, c_r. a) Unscaled per-spin magnetization m_z vs H. b) Scaled per-spin magnetization m_z vs H/c_r^2, in accordance with Eq. (4.2).

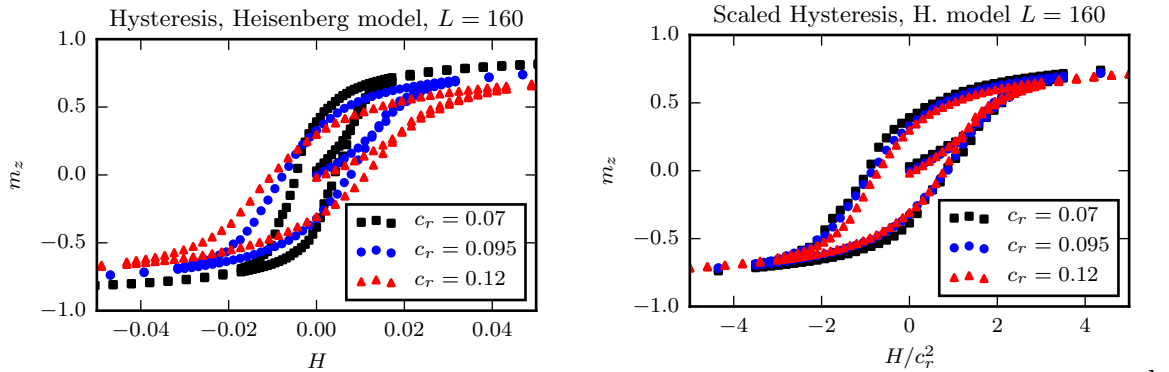

a b

Figure 4.5: Hysteresis loops for the $3d$ Heisenberg model with dilute strong random field for different concentration of the random-field sites, c_r. a) Unscaled per-spin magnetization m_z vs H. b) Scaled per-spin magnetization m_z vs H/c_r^2, in accordance with Eq. (4.2).

initially oriented in one direction) always has non-zero magnetization. This is an indication of metastability and glassy behavior caused by the dilute random field. There may be as little profit in looking for the "needle-in-the-haystack" ground state of such a system as in looking for the ground-state configuration of domains of a conventional permanent magnet with a macroscopic number of defects that pin domain walls. We, therefore, turn to the magnetic hysteresis as a measure of metastability. We compute the magnetization per spin m_z induced by the field applied in the Z-direction. Hysteresis loops for XY and Heisenberg models are shown in Figs. 4.5 and 4.4. The scaling in terms of H/c_r^2 is very good, implying that the coercive field and the area of the hysteresis loop roughly scale as c_r^2.

4.2 Qualitative Explanation

Our findings can be explained in a simple manner by employing the Imry-Ma argument given in Section 1.1. It is convenient to rescale the problem to subvolumes of size $r_h \sim 1/c_r^{1/3}$, which represents the average distance between the random-field sites. In the lattice units, the effective random field per spin inside such a volume is of order $h_{r_h} \sim h/r_h^3$. Our rescaled Hamiltonian is then

$$\int d^3r \, \frac{Ja^2}{2} \left(\boldsymbol{\nabla} \cdot \mathbf{S}\right)^2 - \frac{h}{r_h^3} \mathbf{n} \cdot \mathbf{S}. \tag{4.1}$$

Plugging in these rescaled parameters into Eq. (1.9), we find $R_f \propto r_h^3 (J/h)^2 \propto 1/c_r$, in accordance with our numerical results.

Plugging the same rescaled parameters from Eq. (4.1) into Eq. (1.12), we find

$$H_c \propto \frac{h^4 c_r^2}{J^3 a^6} \tag{4.2}$$

This scaling of the coercive field and, consequently, of the area of the hysteresis loop is in agreement with our numerical results.

4.3 Discussion

Our model directly applies to a ferromagnet with magnetic impurities having strong single-ion anisotropy that freezes their spins in random directions. We assume that such impurities interact strongly via ferromagnetic or antiferromagnetic exchange with the surrounding spins. Note that every magnetic system also has relativistic interactions, such as dipole-dipole and magneto-crystalline anisotropy terms in the Hamiltonian, that would break the system into domains even in the absence of the spin impurities generating strong random fields[54]. However, for sufficiently large concentration of magnetic impurities the formation of the short-range order would be dominated by their strong exchange interaction with the surrounding spins rather than by the weak relativistic interactions in the system. In general, magnetic impurities must be of practical significance if the short-range-order ferromagnetic correlation length, $R_f \propto 1/c_r$, that they are responsible for, is smaller than the would-be average domain size without the magnetic impurities.

While the spin problem does not map exactly onto the flux-lattice problem or the CDW problem (see discussion of these issues in, e.g., Refs. [47] and [11]), all three problems are conceptually similar. Consequently, our study supports statements of Refs. [10] and [11] that the correlation length in the CDW problem with diluted strong pinning centers is large compared to the average distance between the centers. Our prediction for the correlation length is $R_f \sim 1/c_r \gg r_h \sim 1/c_r^{1/3}$. It would be interesting to test this prediction in $NbSe_2$. It can also be tested on flux lattices that are pinned by strong pinning centers with concentration $c_r \ll 1$. Scaling of the critical current as $j_c \sim 1/R_f^2$ [4] would then imply $j_c \propto c_r^2$.

Chapter 5

Scaling of coercivity in a 3d random anisotropy model

5.1 Introduction

The random anisotropy model was introduced by Harris, Plischke, and Zuckermann[56] to describe magnetic properties of amorphous ferromagnets. The problem is subtle when local magnetic anisotropy is weak compared to the exchange interaction, which is usually the case due to the relativistic nature of the anisotropy. In this case the exchange interaction creates extended ferromagnetic ordering.

In a crystalline ferromagnet the ordered regions would correspond to ferromagnetic domains separated by thin domain walls, with the magnetization inside the domains aligned with the directions of the global anisotropy axes. If one neglects the magnetic dipole interaction, the ground state corresponds to the infinite size of the domain, that is, to the global ferromagnetic ordering. It is the magnetic dipole interaction that breaks ferromagnetic crystal into domains, with the ground state corresponding to zero total magnetic moment. In

This chapter is based on work originally presented in Ref. [55]

practice, however, pinning of domain walls by disorder results in the magnetic hysteresis that permits permanent magnets.

In a random-anisotropy ferromagnet the global directions of the anisotropy are absent, and the analysis given in Section 1.1 applies. For any practical purpose, this makes random field and random anisotropy systems not very different from a conventional ferromagnet, having high metastability and magnetic hysteresis that only disappears at sufficiently high temperature or exponentially long times.

Similarly to the random field model, we would expect the formation of the Imry-Ma state to require the creation of topological defects, although there are peculiarities which we will discuss in Section 5.4.

In this chapter we study the random anisotropy Heisenberg model on lattices in excess of ten million spins. The emphasis is on measurable quantities, such as magnetic hysteresis, the coercive field, and their dependence on the anisotropy strength and the size of the volume inside which the anisotropy axes are correlated. The latter is relevant to the magnets sintered from randomly oriented nanoscopic ferromagnetic grains. We find very strong dependence of the magnetic properties on parameters, which we believe is important for synthesizing materials with desired magnetic properties.

This chapter is structured as follows: The model is formulated in Section 5.2, where some analytical results are also obtained. The numerical method and results are presented in Section 5.3. We begin by analyzing the case of site disorder. Section 5.3.1 compares short-range correlations computed numerically with analytical results, and provides spin-spin correlation functions for different initial conditions. Section 5.3.2 presents computed hysteresis curves and obtains their scaling with the strength of the random anisotropy. The role of hedgehogs in the magnetic state is discussed in Section 5.3.3. Section 5.3.4 presents numerical results and their interpretation in the random anisotropy system that has short range correlations in the distribution of the anisotropy axes. Section 5.4 contains some final

remarks and suggestions for experiment.

5.2 Model and Analytical Results

The three-dimensional Heisenberg model with random anisotropy is described by the Hamiltonian

$$\mathcal{H} = -\frac{J}{2}\sum_{i,j}\mathbf{s}_i \cdot \mathbf{s}_j - D_R\sum_i(\mathbf{n}_i \cdot \mathbf{s}_i)^2 - \mathbf{H}\cdot\sum_i \mathbf{s}_i, \tag{5.1}$$

where the first sum is over nearest neighbors, $\mathbf{s}_i$ is a three component spin of constant length s, $\mathbf{H}$ is the external field, D_R is the strength of the random anisotropy, and $\mathbf{n}_i$ is a three-component unit vector having random direction at each lattice site. We assume ferromagnetic exchange, $J > 0$. The factor of $1/2$ in front of the first term is needed to count the exchange interaction Js^2 between each pair of spins once. In our numerical work we consider a cubic lattice. For the real atomic lattice of cubic symmetry the single-ion anisotropy of the form $-(\mathbf{n}\cdot\mathbf{s})^2$ would be absent, the first non-vanishing anisotropy terms would be of the form $s_x^2 s_y^2 + s_x^2 s_z^2 + s_y^2 s_z^2$. However, in our case the choice of a cubic lattice is merely a computational tool that should not affect our conclusions.

In a cubic lattice the effective exchange field acting on each spin is $6Js$ due to six nearest neighbors. In our model it competes with the anisotropy field of strength $2sD_R$. The case of a large random anisotropy, $2sD_R \gg 6Js$, that is, $D_R \gg 3J$, is obvious, corresponding to a system of weakly interacting randomly oriented single-domain particles. At $T = 0$ each spin aligns with the local $\mathbf{n}$. At $T = 0$, due to the two equivalent directions along the easy axis, the system possesses magnetic hysteresis with a coercive field, H_C, of the order of the local anisotropy field $H_C \propto 2sD_R$. For the more subtle case of weak random anisotropy, $D_R \ll 3J$, correlations would be expected to follow the predictions of the Imry-Ma argument (Section 1.1), and $R_f/a \propto (3J/D_R)^2$, in accordance with Eq. (1.9).

This famous argument[2] provides an estimate of the size of the Imry-Ma domain, i.e. the

distance R_f on which the magnetization rotates by a significant angle. It leaves open the question whether the ground state of the random anisotropy system possesses a non-zero magnetization M. Even if it does, as is the case in the domain state of a conventional macroscopic ferromagnet, the state with $M = 0$ may have no practical significance because the presence of topological defects and their pinning by disorder will always result in metastability and magnetic hysteresis. The coercive field in the weak random anisotropy case must be proportional to $D_{\rm eff}$ on the scale R_f, which gives $H_C \propto D_R^4/J^3$. The proportionality of H_C to the fourth power of D_R gives a very soft magnet in the limit of small D_R. This can be extended to the limit of a Heisenberg ferromagnet with no anisotropy at all, which has infinite susceptibility.

The qualitative arguments presented above can be refined using a continuous field theory version of the Hamiltonian given in Eq. (5.1),

$$\mathcal{H} = \int d^3r \left[\frac{\alpha}{2} (\partial_\mu \mathbf{S}) \cdot (\partial_\mu \mathbf{S}) - \frac{\beta_R}{2} (\mathbf{n} \cdot \mathbf{S})^2 - \mathbf{H} \cdot \mathbf{S} \right], \tag{5.2}$$

where $\alpha = Ja^5$, $\beta_R = 2D_R a^3$, $\mathbf{S}(\mathbf{r})$ is a three-component spin field of length $S_0 = s/a^3$, and $\mathbf{n}(\mathbf{r})$ is a three-component random field of unit length. Adding a Lagrange multiplier term, $-\int d^3r\, \lambda(\mathbf{r}) \mathbf{S}^2$, to Eq. (5.2) which accounts for the $\mathbf{S}^2(\mathbf{r})$ being constant, one obtains the following equation for the extremal $\mathbf{S}(\mathbf{r})$ configurations:

$$\alpha \nabla^2 \mathbf{S} + \beta \mathbf{n} (\mathbf{n} \cdot \mathbf{S}) + 2\lambda \mathbf{S} = 0 \tag{5.3}$$

Multiplying by $\mathbf{S}_0$, one obtains an equation for λ. At $R \ll R_f$ it gives

$$\alpha \nabla^2 \mathbf{S} = -\beta \mathbf{n} (\mathbf{S} \cdot \mathbf{n}) + \frac{\beta}{S_0^2} \mathbf{S} (\mathbf{S} \cdot \mathbf{n})^2 \tag{5.4}$$

$$\mathbf{S}(\mathbf{r}) = -\frac{\beta}{\alpha}\int d^3r' G(\mathbf{r}-\mathbf{r}') \times \left\{ \mathbf{n}(\mathbf{r}')[\mathbf{S}(\mathbf{r}')\cdot\mathbf{n}(\mathbf{r}')] - \frac{1}{S_0^2}\mathbf{S}(\mathbf{r}')[\mathbf{S}(\mathbf{r}')\cdot\mathbf{n}(\mathbf{r}')]^2 \right\} \tag{5.5}$$

where $G(\mathbf{r}) = -1/(4\pi|\mathbf{r}|)$ is the Green function of the Laplace equation. Then

$$\frac{1}{2S_0^2}\langle[\mathbf{S}(\mathbf{r}_1)-\mathbf{S}(\mathbf{r}_2)]^2\rangle = 1 - \frac{1}{S_0^2}\langle\mathbf{S}(\mathbf{r}_1)\cdot\mathbf{S}(\mathbf{r}_2)\rangle = \\ = \frac{\beta^2}{2\alpha^2}\int d^3r' \int d^3r''[G(\mathbf{r}_1-\mathbf{r}') - G(\mathbf{r}_2-\mathbf{r}')][G(\mathbf{r}_1-\mathbf{r}'') - G(\mathbf{r}_2-\mathbf{r}'')]\langle\mathbf{u}(\mathbf{r}')\cdot\mathbf{u}(\mathbf{r}'')\rangle \tag{5.6}$$

where $\mathbf{u} = \mathbf{n}(\boldsymbol{\sigma}\cdot\mathbf{n}) - \boldsymbol{\sigma}(\boldsymbol{\sigma}\cdot\mathbf{n})^2$.

At $R_f \gg a$ the direction of $\mathbf{S}$ is roughly uncorrelated with the direction of $\mathbf{n}$ at the same lattice site. This gives

$$\langle\mathbf{u}(\mathbf{r}')\cdot\mathbf{u}(\mathbf{r}'')\rangle = \langle n'_\alpha n'_\beta n''_\gamma n''_\delta\rangle \times \sigma'_\beta\sigma''_\delta(\sigma'_\alpha\sigma'_\mu - \delta_{\alpha\mu})(\sigma''_\gamma\sigma''_\mu - \delta_{\gamma\mu})\rangle, \tag{5.7}$$

where $\mathbf{n}' = \mathbf{n}(\mathbf{r}'), \mathbf{n}'' = \mathbf{n}(\mathbf{r}'')$ and the same for $\boldsymbol{\sigma}$. The general form of the anisotropy correlator is

$$n'_\alpha n'_\beta n''_\gamma n''_\delta\rangle = \frac{1}{5}[A(\mathbf{r}',\mathbf{r}'')\delta_{\alpha\beta}\delta_{\gamma\delta} + B(\mathbf{r}',\mathbf{r}'')(\delta_{\alpha\gamma}\delta_{\beta\delta} + \delta_{\alpha\delta}\delta_{\beta\gamma})] \tag{5.8}$$

The condition $\mathbf{n}^2 = 1$ gives $A = B = 1$ at $\mathbf{r}' = \mathbf{r}''$, and $A = 5/3$, $B = 0$ at $|\mathbf{r}' - \mathbf{r}''| \to \infty$. It is easy to see that the A-term in Eq. (5.8) does not contribute to Eq. (5.7). Replacing B with $a^3\delta(\mathbf{r}' - \mathbf{r}'')$, one obtains

$$\frac{1}{2S_0^2}\langle[\mathbf{S}(\mathbf{r}_1)-\mathbf{S}(\mathbf{r}_2)]^2\rangle = 1 - \frac{1}{S_0^2}\langle\mathbf{S}(\mathbf{r}_1)\cdot\mathbf{S}(\mathbf{r}_2)\rangle = \\ = \frac{\beta^2 a^3}{15\alpha^2}\int d^3r[G(\mathbf{r}_1-\mathbf{r}) - G(\mathbf{r}_2-\mathbf{r})]^2 \\ = \frac{\beta^2 a^3}{60\pi\alpha^2}|\mathbf{r}_1-\mathbf{r}_2| = \frac{|\mathbf{r}_1-\mathbf{r}_2|}{R_f} \tag{5.9}$$

at $|\mathbf{r}_1 - \mathbf{r}_2| \ll R_f$, where

$$\frac{R_f}{a} = \frac{60\pi\alpha^2}{\beta^2 a^4} = 15\pi \left(\frac{J}{D_R}\right)^2 \tag{5.10}$$

in accordance with the Imry-Ma argument.

5.3 Numerical Results

Our numerical method follows the one given in Section 1.2. However, unlike the case of the random field model, the overrelaxation given in Eq. (1.15) does not conserve energy. Substituting Eq. (1.15) into the original Random anisotropy Hamiltonian given by Eq. (5.1), we find that the energy with the overrelaxed spin is

$$\mathcal{H}_{i,\text{new}} \approx -mJ\mathbf{s}_i\cdot\mathbf{s}_{\text{ext}} - 2D_R(\mathbf{n}_i\cdot\mathbf{s}_i)^2 - \mathcal{H}_i - D_R\left(\frac{2\mathbf{s}_i\cdot\mathbf{s}_{\text{ext}}}{s_{\text{ext}}^2}\right)^2(\mathbf{n}_i\cdot\mathbf{s}_{\text{ext}})^2 - \frac{2D_R}{s_{\text{ext}}^2}(\mathbf{n}_i\cdot\mathbf{s}_{\text{ext}})(\mathbf{n}_i\cdot\mathbf{s}_i)(\mathbf{s}_i\cdot\mathbf{s}_{\text{ext}}), \tag{5.11}$$

where $\mathbf{s}_{\text{ext}} \equiv \sum_i \mathbf{s}_i/m$, summing over nearest neighbors, with m the number of nearest neighbors. When $R_f \gg a$, nearest neighbor spins will be approximately aligned, and

$$\mathcal{H}_{i,\text{new}} \approx \mathcal{H}_i - \frac{2D_R}{s_{\text{ext}}}\left(\frac{2(\mathbf{n}_i\cdot\mathbf{s}_{\text{ext}})^2}{s_{\text{ext}}} + (\mathbf{n}_i\cdot\mathbf{s}_{\text{ext}})(\mathbf{n}_i\cdot\mathbf{s}_i)\right). \tag{5.12}$$

The first term that is added to the original Hamiltonian is obviously negative. As $\mathbf{s}_i$ and $\mathbf{s}_{\text{ext}}$ are approximately aligned, $\mathbf{n}_i\cdot\mathbf{s}_{\text{ext}}$ and $\mathbf{n}_i\cdot\mathbf{s}_i$ will have the same sign, so $(\mathbf{n}_i\cdot\mathbf{s}_{\text{ext}})(\mathbf{n}_i\cdot\mathbf{s}_i)$ is positive, and the term that contains it keeps the negative sign.

Thus, when the nearest-neighbor spins are approximately aligned, overrelaxation reduces the energy. At each site, we randomly choose between the two processes, and continue do so throughout the lattice, repeating until we reach convergence. This overrelaxation method has been found to produce much faster convergence than the ordinary relaxation. The combination of relaxation and overrelaxation converges to a representative local energy min-

imum that is typical of a glassy system. All our computations are done at zero temperature and therefore are relevant to the hysteretic behavior of the random anisotropy system at temperatures well below the Curie temperature of the local ferromagnetic ordering.

5.3.1 Correlation Functions

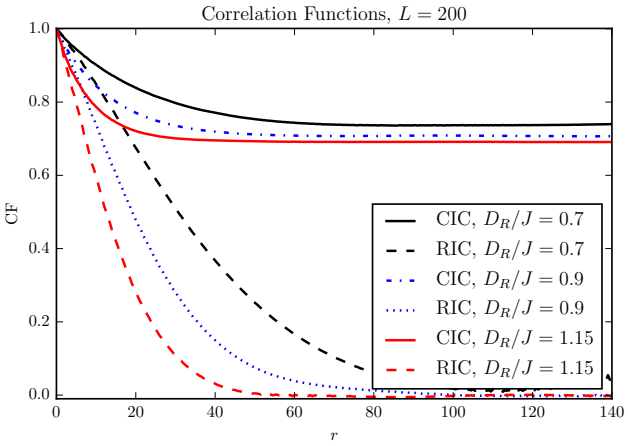

Figure 5.1: Correlation functions from random initial conditions (RIC) and collinear initial conditions (CIC). Full color online.

We have computed spin-spin correlation functions, defined by $CF\,(R) \equiv \langle \mathbf{s}(\mathbf{r}) \cdot \mathbf{s}\,(\mathbf{r} - \mathbf{R})\rangle$. Two initial conditions have been used. Collinear initial conditions (CIC) physically correspond to the state obtained by placing the sample in a strong magnetic field which is then turned off. Random initial conditions (RIC) physically correspond to fast cooling followed by relaxation in zero magnetic field. Correlation functions are shown in Fig. 5.1. As would be expected, the curves differ significantly depending on initial conditions. Under collinear initial conditions, the CF levels off to a finite value, in agreement with the significant magnetization that remains. However, correlations go to zero for random initial conditions, consistent with zero magnetization.

It is interesting to compare the linear decrease of the CF at very small R with the prediction of the analytical theory, $CF = s^2(1 - R/R_f)$. The dependence of R_f on D_R

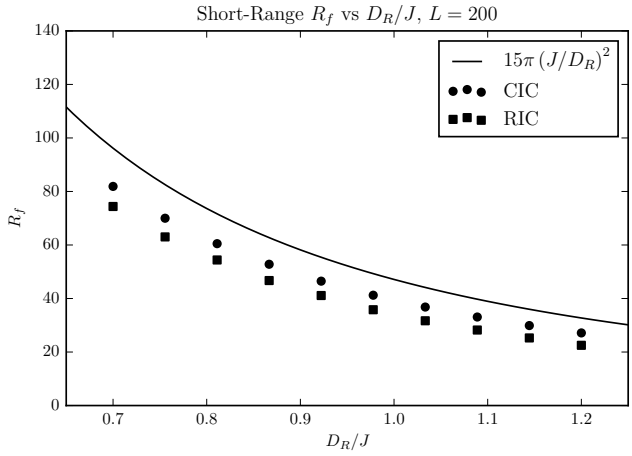

Figure 5.2: Short-range Correlation lengths for CIC and RIC

extracted from the linear dependence of the CF on R at $R \ll R_f$ is shown in Fig. 5.2. It is consistent with Eq. (5.10), although the agreement is not exact. This is not surprising since the analytical theory did not account for topological defects, which we discuss in Section 5.4. At greater R the correlation function for the state obtained from the RIC roughly follows $\exp(-R/R'_f)$ with R'_f given by $R'_f/a \approx 22\,(J/D_R)^2$. While R'_f is slightly shorter than R_f, it also follows the $1/D_R^2$ dependence, in agreement with the Imry-Ma argument.

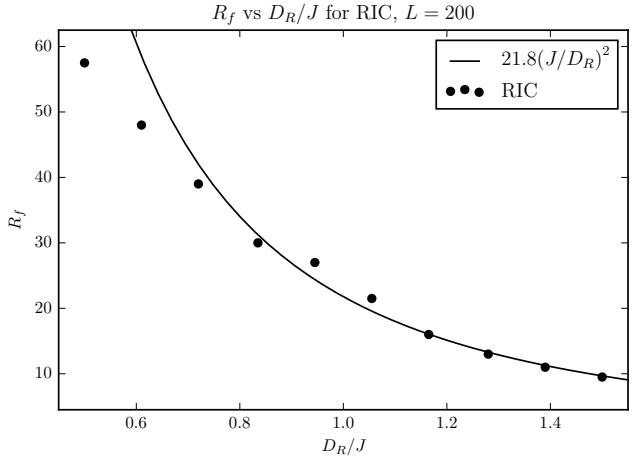

Figure 5.3: Correlation lengths for RIC

5.3.2 Hysteresis

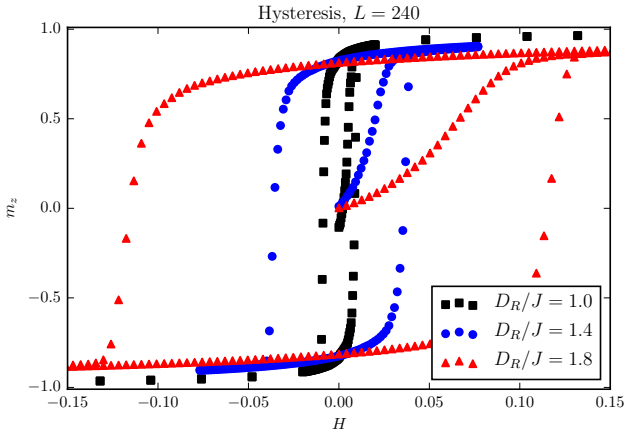

Figure 5.4: Hysteresis curves. Full color online.

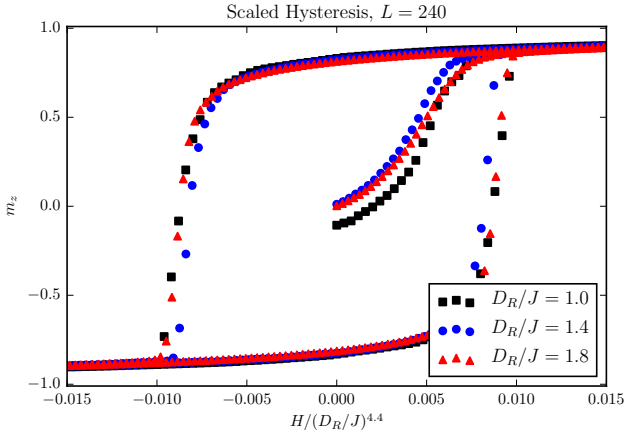

Figure 5.5: Hysteresis curves scaled. Full color online

We have numerically computed hysteresis curves using the above method. The results for different D_R are shown in Fig. 5.4. They can be reasonably well scaled by dividing H by a certain power of D_R as is shown in Fig. 5.5. This scaling allows one to approximate the coercive field, H_C, i.e. the field required to bring magnetization to zero from saturation, by $H_C \approx D_R^{4.4}/118$. The area of the hysteresis loop scales similarly. This is roughly consistent with the expectation that H_C scales as the fourth power of D_R, given by Eq. (1.12), although the agreement is not precise.

5.3.3 Hedgehogs

$3d$ Heisenberg model has topological defects – "hedgehogs"– which correspond to the magnetization vector field going into a point or sticking out of a point. Hedgehogs possess ± 1 topological charge and thus appear in pairs. In the absence of random anisotropy, hedgehogs and anti-hedgehogs would be attracted to each other and would annihilate. However, random anisotropy can stabilize hedgehogs even at $T = 0$. Random initial conditions automatically introduce hedgehogs. Relaxation from RIC annihilates some of the hedgehog pairs but leaves the system with a finite residual number of hedgehogs which depends on the strength of the random anisotropy. This must be one of the reasons why predictions of the continuous model deviate from numerical results.

We can find hedgehogs in our computed states using a simple method: we look for points between lattice sites where spins on opposite sides of the point are aligned in opposite directions. This method consistently finds hedgehogs; all other configurations that satisfy this condition are forbidden by theory, so there is no risk for false positives. Except for very high strengths of the random anisotropy, collinear initial conditions generally do not produce any singularities. Random initial conditions, however, do produce singularities. Fig. 5.6 shows the density of hedgehogs, ρ_H, i.e. the ratio between the number of points where hedgehogs have been found and the total number of sites, versus the strength of the random anisotropy, D_R.

We have found that $\rho_H \approx (0.19 D_R/J)^6$. Combining this result with Eq. (5.10), we obtain

$$\rho_H \approx \frac{2.1}{\frac{4}{3}\pi (R_f/a)^3}, \tag{5.13}$$

i.e. there are approximately two Hedgehogs per Imry-Ma domain. This finding is in accordance with the topological argument presented in Chapter 2: the Imry-Ma state with zero total magnetization requires singularities at $n < d + 1$, where n is the number of spin

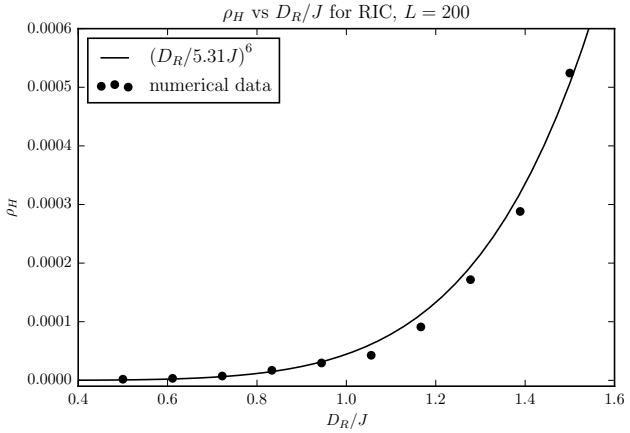

Figure 5.6: Hedgehog density vs D_R.

components and d is dimensionality of space.

5.3.4 Correlated disorder

So far we have studied the site disorder, i.e. the direction of the anisotropy was chosen randomly at each lattice site. Meanwhile, amorphous and sintered magnets would have anisotropy axes correlated on some scale $R_a > a$, and the coercive field will be given by Eq. (1.12). This sixth power dependence of the coercive field on the grain size is confirmed by numerical results. These numerical results are obtained by using cubic correlated chunks, where all sites within a cubic region with volume R_a^3 have aligned anisotropy axes. This corresponds to the physical conditions in sintered magnets. Fig. 5.7 shows the dependence of H_C on R_a for $R_a = a, 2a, 3a, 4a, 5a$. Note that R_f is proportional to the inverse third power of R_a, which invalidates the condition $R_a \ll R_f$ very fast with increasing R_a, limiting numerical studies of a finite-size system to just a few grain sizes.

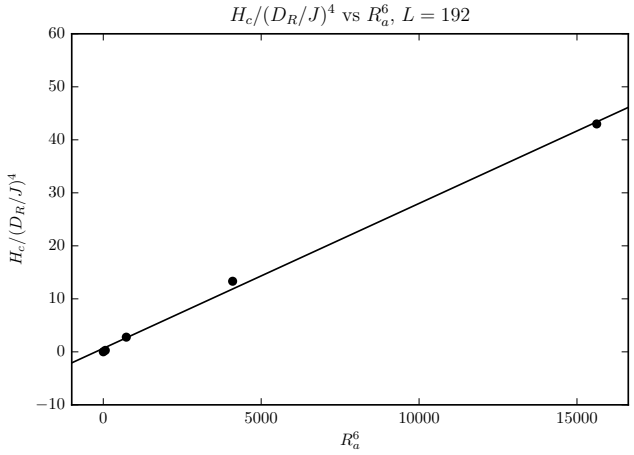

Figure 5.7: The dependence of the coercive field on the size of the grain, R_a. The points correspond to $R_a/a = 1, 2, 3, 4, 5$.

5.4 Discussion

Using $3d$ lattices containing over 10 million spins, we have numerically studied the magnetic properties of the random-anisotropy Heisenberg model in the limit when the anisotropy is sufficiently weak compared to the exchange to provide a ferromagnetic correlation length that is greater than the scale on which anisotropy axes are correlated. This limit will be satisfied by many amorphous magnets, as well as by sintered magnets in which the size of the grain, R_a, is sufficiently small. Taking $R_f/a = 15\pi(a/R_a)^3(J/D_R)^2$ in accordance with our analytical and numerical results, one obtains that the condition $R_a \ll R_f$ requires $R_a/a \ll (J/D_R)^{1/2}$. Had D_R been the magneticrystalline anisotropy, $(J/D_R)^{1/2}a$ would have represented the scale of the domain wall width. Consequently, if the magnet was sintered from ferromagetic nanocrystals, the condition $R_a \ll R_f$ would correspond to the condition that the size of the nanocrystal was small compared to the domain wall width in the magnetic material. This is practically feasible and, in fact, reflects the direction in which the magnetic industry is going.

Under the above condition, we found, in accordance with theoretical expectation, that

the coercive field and the area of the hysteresis loop roughly scale as D_R^4 and R_a^6. This strong dependence on parameters shows that decreasing D_R and R_a by even a small factor could drastically reduce the coercive field, paving the way to extremely soft magnetic materials. One obstacle could be the coherent anisotropy which is inevitably present in any sample due to its non-spherical shape and/or the anisotropy of the process of sample preparation. Let such anisotropy have strength D_C. Its effect on the magnetic state will be small if it is weak compared to the effective anisotropy stemming from D_R. The latter, as our theoretical argument suggests and numerical work confirms, scales as $D_{\text{eff}} \sim D_R^4/J^3$. Consequently, the condition $D_C \ll D_{\text{eff}}$ translates into $D_C/J \ll (D_R/J)^4$. Thus, in the case of a weak random anisotropy, a much weaker coherent anisotropy would destroy the softness of the magnet and will convert it into a more conventional ferromagnet with domain walls of the width $\sim (J/D_C)^{1/2}$ pinned by disorder.

An interesting question is the physical origin of metastability. We have seen that, similar to the random field model,[38] the metastability comes in large part from hedgehogs, whose concentration strongly depends on D_R and corresponds to about two hedgehogs per volume of size R_f. However, there is a difference from the random-field model. In a random field system the metastability and hysteresis disappear for $n > d + 1$ when topological defects are absent. In contrast, magnetic anisotropy in the random anisotropy model introduces bistability, creating topological defects – domain walls – regardless of the relation between n and d. In principle, one can think of domain walls of width $\sim (J/D_{\text{eff}})^{1/2}a$. However, substitution of $D_{\text{eff}} \sim D_R^4/J^3$ into this expression gives a width, $\sim (J/D_R)^2 a$, which scales as R_f, making the concept of a domain wall separating domains useless. Nevertheless, the topology of the random-anisotropy model remains different from the topology of the random-field model. We observed this by numerically studying the $3d$ random-anisotropy model with a five-component spin. Although the agreement with analytical results becomes more precise when the hedgehogs are absent, hysteresis persists, unlike the behavior found in the random

field model.

Chapter 6

Conclusion

Throughout this work, we have explored a wide range of models with various forms of quenched randomness. We have numerically found local energy minima on lattices of between forty thousand and ten million spins, and explored the correlation functions of these energy minima, along with hysteresis created by sweeping an external field. In Chapter 2, we showed what became our guiding principle in later chapters: systems with quenched randomness are dominated by topological effects. We found that random field models with dimensionality $n > d + 1$ show behavior that is perfectly consistent with the Imry-Ma picture given in Section 1.1, but models with $n < d + 1$ models have topological defects that complicate the picture.

We then focused in on a particular random field model, the XY model, and studied the details of this complicated picture. We looked at two metastable states of this model, one where we found correlations are determined by the density of pinned topological charges, and one that looks like the Imry-Ma picture at short ranges, but has some long range order. Hysteresis curves also showed evidence of metastability, with domains persisting in the hysteresis curve which require the creation of topological defects to destroy.

A dilute random field model was studied, and we focused on some of aspects that are

most experimentally applicable. We found that both the short-range correlation functions and the scaling of the hysteresis curves are consistent with the Imry-Ma picture, despite the complications from topology.

Finally, we looked at a random anisotropy model. This model adds the complication of domain walls to the topological picture, but we find that the hysteresis cures and short-range correlations are still consistent with the Imry-Ma picture.

The models studied here do not cover the infinite number of possible models with quenched randomness, and there are probably a large number remaining that are physically relevant However, our conclusions show that the topology of the system is very important, and that random models with $n < d + 1$ can be expected to have extensive metastability. Despite these complicating factors, the Imry-Ma picture remains a good starting point. In all of the systems we have studied, there is some aspect of the Imry-Ma picture that remains relevant, most notably the scaling of the hysteresis curve.

References

1. Larkin, A. I. Effect of inhomogeneities on the structure of the mixed state of superconductors. *Sov. Phys. JETP* **31,** 784 (4 1970).
2. Imry, Y. & Ma, S.-k. Random-Field Instability of the Ordered State of Continuous Symmetry. *Phys. Rev. Lett.* **35,** 1399–1401 (21 1975).
3. Aizenman, M. & Wehr, J. Rounding of first-order phase transitions in systems with quenched disorder. *Phys. Rev. Lett.* **62,** 2503–2506 (21 1989).
4. Blatter, G., Feigel'man, M. V., Geshkenbein, V. B., Larkin, A. I. & Vinokur, V. M. Vortices in high-temperature superconductors. *Rev. Mod. Phys.* **66,** 1125–1388 (4 1994).
5. Grier, D. G. *et al.* Translational and bond-orientational order in the vortex lattice of the high-T_c superconductor $Bi_{2.1}Sr_{1.9}Ca_{0.9}Cu_2O_{8+\delta}$. *Phys. Rev. Lett.* **66,** 2270–2273 (17 1991).
6. Klein, T. *et al.* A Bragg glass phase in the vortex lattice of a type II superconductor. *Nature* **413,** 404–406 (6854 2001).
7. Fukuyama, H. & Lee, P. A. Dynamics of the charge-density wave. I. Impurity pinning in a single chain. *Phys. Rev. B* **17,** 535–541 (2 1978).
8. Lee, P. A. & Rice, T. M. Electric field depinning of charge density waves. *Phys. Rev. B* **19,** 3970–3980 (8 1979).
9. Grüner, G. The dynamics of charge-density waves. *Rev. Mod. Phys.* **60,** 1129–1181 (4 1988).
10. Okamoto, J.-i., Arguello, C. J., Rosenthal, E. P., Pasupathy, A. N. & Millis, A. J. Experimental Evidence for a Bragg Glass Density Wave Phase in a Transition-Metal Dichalcogenide. *Phys. Rev. Lett.* **114,** 026802 (2 2015).
11. Okamoto, J.-i. & Millis, A. J. *Effect of dilute, strongly pinning impurities on charge density waves* 2014.
12. Efetov, K. B. & Larkin, A. I. Charge-density wave in a random potential. *Sov. Phys. JETP* **45,** 1236–1241 (6 1977).
13. Nattermann, T. Scaling approach to pinning: Charge density waves and giant flux creep in superconductors. *Phys. Rev. Lett.* **64,** 2454–2457 (20 1990).

14. Fishman, S. & Aharony, A. Random field effects in disordered anisotropic antiferromagnets. *Journal of Physics C: Solid State Physics* **12,** L729 (1979).

15. Chudnovsky, E. M. Instanton Glass Generated by Noise in a Josephson-Junction Array. *Phys. Rev. Lett.* **103,** 137001 (13 2009).

16. Seshadri, R. & Westervelt, R. M. Statistical mechanics of magnetic bubble arrays. I. Topology and thermalization. *Phys. Rev. B* **46,** 5142–5149 (9 1992).

17. Seshadri, R. & Westervelt, R. M. Statistical mechanics of magnetic bubble arrays. II. Observations of two-dimensional melting. *Phys. Rev. B* **46,** 5150–5161 (9 1992).

18. Volovik, G. On Larkin-Imry-Ma State of 3He-A in Aerogel. English. *Journal of Low Temperature Physics* **150,** 453–463. ISSN: 0022-2291 (2008).

19. Li, J. I. A., Pollanen, J., Zimmerman, A. M., Gannon, C. A. C. W. J. & Halperin, W. P. The superfluid glass phase of 3He-A. *Nature Physics* **9,** 775–779 (2013).

20. Patterson, J. D., Gruzalski, G. R. & Sellmyer, D. J. Effect of random anisotropy on magnetic properties of amorphous systems. *Phys. Rev. B* **18,** 1377–1390 (3 1978).

21. Chudnovsky, E. M. A theory of two-dimensional amorphous ferromagnet. *Journal of Magnetism and Magnetic Materials* **40,** 21–26. ISSN: 0304-8853 (1983).

22. Chudnovsky, E. M. & Serota, R. Magnetic properties of solids with small random anisotropy. *Journal of Magnetism and Magnetic Materials* **43,** 48–52. ISSN: 0304-8853 (1984).

23. Chudnovsky, E. M. & Serota, R. A. Spin-glass and ferromagnetic states in amorphous solids. *Phys. Rev. B* **26,** 2697–2699 (5 1982).

24. Pelcovits, R., Pytte, E. & Rudnick, J. Spin-Glass and Ferromagnetic Behavior Induced by Random Uniaxial Anisotropy. *Phys. Rev. Lett.* **40,** 476–479 (7 1978).

25. Cardy, J. L. & Ostlund, S. Random symmetry-breaking fields and the XY model. *Phys. Rev. B* **25,** 6899–6909 (11 1982).

26. Villain, J. & Fernandez, J. Harmonic system in a random field. English. *Zeitschrift für Physik B Condensed Matter* **54,** 139–150. ISSN: 0722-3277 (1984).

27. Feldman, D. E. Quasi-long-range order in the random anisotropy Heisenberg model: Functional renormalization group in $4 - \epsilon$ dimensions. *Phys. Rev. B* **61,** 382–390 (1 2000).

28. Kierfeld, J., Nattermann, T. & Hwa, T. Topological order in the vortex-glass phase of high-temperature superconductors. *Phys. Rev. B* **55,** 626–629 (1 1997).

29. Korshunov, S. E. Replica symmetry breaking in vortex glasses. *Phys. Rev. B* **48,** 3969–3975 (6 1993).

30. Giamarchi, T. & Le Doussal, P. Elastic theory of pinned flux lattices. *Phys. Rev. Lett.* **72,** 1530–1533 (10 1994).

31. Giamarchi, T. & Le Doussal, P. Elastic theory of flux lattices in the presence of weak disorder. *Phys. Rev. B* **52,** 1242–1270 (2 1995).

32. Bogner, S., Emig, T., Taha, A. & Zeng, C. Test of replica theory: Thermodynamics of two-dimensional model systems with quenched disorder. *Phys. Rev. B* **69,** 104420 (10 2004).

33. Orland, H. & Shapir, Y. A Disorder-Dependent Variational Method Without Replicas: Application to the Random Phase Sine-Gordon Model. *EPL (Europhysics Letters)* **30,** 203 (1995).

34. Garel, T., Iori, G. & Orland, H. Variational study of the random-field XY model. *Phys. Rev. B* **53,** R2941–R2944 (6 1996).

35. Dieny, B. & Barbara, B. *XY* model with weak random anisotropy in a symmetry-breaking magnetic field. *Phys. Rev. B* **41,** 11549–11556 (16 1990).

36. Adler, S. L. Over-relaxation method for the Monte Carlo evaluation of the partition function for multiquadratic actions. *Phys. Rev. D* **23,** 2901–2904 (12 June 1981).

37. Chen, K. & Landau, D. P. Spin-dynamics study of the dynamic critical behavior of the three-dimensional classical Heisenberg ferromagnet. *Phys. Rev. B* **49,** 3266–3274 (5 Feb. 1994).

38. Proctor, T. C., Garanin, D. A. & Chudnovsky, E. M. Random Fields, Topology, and the Imry-Ma Argument. *Phys. Rev. Lett.* **112,** 097201 (9 2014).

39. Ziman, J. M. *Models of Disorder* (Cambridge University Press, Cambridge, England, 1970).

40. Chudnovsky, E. M. & Tejada, J. *Lectures on Magnetism* (Rinton Press, Princeton, New Jersey, 2006).

41. Garanin, D. A., Chudnovsky, E. M. & Proctor, T. Random field *xy* model in three dimensions. *Phys. Rev. B* **88,** 224418 (22 2013).

42. Cai, L., Chudnovsky, E. M. & Garanin, D. A. Collapse of skyrmions in two-dimensional ferromagnets and antiferromagnets. *Phys. Rev. B* **86,** 024429 (2 2012).

43. Aizenman, M. & Wehr, J. Rounding effects of quenched randomness on first-order phase transitions. English. *Communications in Mathematical Physics* **130,** 489–528. ISSN: 0010-3616 (1990).

44. Stanley, H. E. Spherical Model as the Limit of Infinite Spin Dimensionality. *Phys. Rev.* **176,** 718–722 (2 1968).

45. Garanin, D. A., Chudnovsky, E. M. & Proctor, T. The role of vortices in the three-dimensional random-field xy model. *EPL (Europhysics Letters)* **103,** 67009 (2013).

46. Nattermann, T. & Scheidl, S. Vortex-glass phases in type-II superconductors. *Advances in Physics* **49,** 607–704 (2000).

47. Gingras, M. J. P. & Huse, D. A. Topological defects in the random-field XY model and the pinned vortex lattice to vortex glass transition in type-II superconductors. *Phys. Rev. B* **53,** 15193–15200 (22 1996).

48. Fisher, D. S. Stability of Elastic Glass Phases in Random Field XY Magnets and Vortex Lattices in Type-II Superconductors. *Phys. Rev. Lett.* **78,** 1964–1967 (10 1997).

49. Perret, A., Ristivojevic, Z., Le Doussal, P., Schehr, G. & Wiese, K. J. Super-Rough Glassy Phase of the Random Field XY Model in Two Dimensions. *Phys. Rev. Lett.* **109,** 157205 (15 Oct. 2012).

50. Aharony, A. & Pytte, E. Low-temperature scaling for systems with random fields and anisotropies. *Phys. Rev. B* **27,** 5872–5874 (9 1983).

51. Garanin, D. A. & Chudnovsky, E. M. Ordered vs. disordered states of the random-field model in three dimensions. *The European Physical Journal B* **88,** 1–19 (2015).

52. Zeng, C., Leath, P. L. & Fisher, D. S. Absence of Two-Dimensional Bragg Glasses. *Phys. Rev. Lett.* **82,** 1935–1938 (9 Mar. 1999).

53. Proctor, T. C. & Chudnovsky, E. M. Effect of a dilute random field on a continuous-symmetry order parameter. *Phys. Rev. B* **91,** 140201 (14 2015).

54. Lifshitz, E. M. & Pitaevskii, L. P. *Course of Theoretical Physics: Volume 9: Statistical Physics Part 2: Theory of the COndensed State* (Pergamon Press, Oxford, England, 1980).

55. Proctor, T., Chudnovsky, E. & Garanin, D. Scaling of coercivity in a 3d random anisotropy model. *Journal of Magnetism and Magnetic Materials* **384,** 181–185. ISSN: 0304-8853 (2015).

56. Harris, R., Plischke, M. & Zuckermann, M. New Model for Amorphous Magnetism. *Phys. Rev. Lett.* **31,** 160–162 (3 1973).